Oceanologia 66 (2024) 111—138

Available online at www.sciencedirect.com

ScienceDirect

journal homepage: www.journals.elsevier.com/oceanologia

ORIGINAL RESEARCH ARTICLE

Submarine groundwater discharge into a semi-enclosed coastal bay of the southern Baltic Sea: A multi-method approach

Cátia Milene Ehlert von Ahn[a,*], Olaf Dellwig[a], Beata Szymczycha[b], Lech Kotwicki[b], Jurjen Rooze[a,j], Rudolf Endler[c], Peter Escher[a,d], Iris Schmiedinger[a], Jürgen Sültenfuß[e], Magdalena Diak[b], Matthias Gehre[f], Ulrich Struck[g], Susan Vogler[a], Michael Ernst Böttcher[a,h,i,*]

[a] *Geochemistry & Isotope Biogeochemistry, Leibniz Institute for Baltic Sea Research (IOW), Warnemünde, Germany*
[b] *Institute of Oceanology, Polish Academy of Sciences (IOPAN), Sopot, Poland*
[c] *Marine Geophysics, Leibniz Institute for Baltic Sea Research (IOW), Warnemünde, Germany*
[d] *current address: Ecoandmore Freiburg, Germany*
[e] *Institute of Environmental Physics, University of Bremen, Bremen, Germany*
[f] *Department of Isotope Biogeochemistry, Helmholtz Centre for Environmental Research (UFZ), Leipzig-Halle, Germany*
[g] *Free University Museum for Natural History, Berlin, Germany*
[h] *Marine Geochemistry, University of Greifswald, Greifswald, Germany*
[i] *Interdisciplinary Faculty, University of Rostock, Rostock, Germany*
[j] *Department of Physical Oceanography and Instrumentation, Leibniz Institute for Baltic Sea Research (IOW), Warnemünde, Germany*

Received 28 February 2023; accepted 10 January 2024
Available online 2 February 2024

KEYWORDS
Stable isotopes;
Radium isotopes;
Acoustic survey;
Diagenesis;
Gulf of Gdańsk;
Puck Bay

Abstract The present study aims to understand the impact of submarine groundwater discharge (SGD) on a coastal area with different lithology and degrees of SGD. Sampling campaigns took place in Puck Bay and the Gulf of Gdańsk, southern Baltic Sea encompassing years between 2009 and 2021. The methodological approach combined geophysical characterization of the surface sediments with detailed spatial and temporal (isotope) biogeochemical investigations of pore and surface waters, and was supported by nearshore groundwater and river surveys. Acoustic investigations identified areas of disturbance that may indicate zones of pref-

* Corresponding authors at: Geochemistry & Isotope Biogeochemistry, Leibniz Institute for Baltic Sea Research (IOW), Warnemünde, Germany.
E-mail addresses: catia.vonahn@io-warnemuende.de (C.M. Ehlert von Ahn), michael.boettcher@io-warnemuende.de (M.E. Böttcher).
Peer review under the responsibility of the Institute of Oceanology of the Polish Academy of Sciences.

Production and hosting by Elsevier

https://doi.org/10.1016/j.oceano.2024.01.001

erential SGD release. The composition of porewater and the differences in the bay's surface waters disclosed SGD as common phenomenon in the study area. Regional SGD was estimated through a radium mass balance. Local estimation of SGD, based on porewater profiles, revealed highest SGD fluxes at the sandy shoreline, but relatively low elemental fluxes. Though SGD was low at the muddy sites corresponding elemental fluxes of nutrients and dissolved carbon exceeded those determined at the sandy sites due to intense diagenesis in the top sediments. SGD appears to be sourced from different freshwater endmembers; however, diagenesis in surface sediments substantially modified the composition of the mixed solutions that are finally discharged to coastal waters. Overall, this study provides a better understanding of the SGD dynamics in the region by a multi-approach and emphasizes the need to understand the processes occurring at the sediment-water interface when estimating SGD.

1. Introduction

Coastal regions are ecosystems subject to intense and dynamic water and elemental fluxes. In addition to surface water discharge, the role of submarine groundwater discharge (SGD) acting as a potential source and carrier of dissolved substances in the coastal ocean has attracted increasing interest from the scientific community over the last decades (Böttcher et al., 2024; Mayfield et al., 2021; Moore, 1996, 2010; Santos et al., 2021; Taniguchi et al., 2002; Zektzer et al., 1973). The term SGD covers a wide range of processes, compositions and origins, including not only the direct discharge of fresh groundwater but also a mixture with recirculated saline porewater through permeable surface sediments (Burnett et al., 2003; Church, 1996; Taniguchi et al., 2002), the quantitative contribution to the water flux across the land-sea interface belonging to the still open questions in hydrology (Blöschl et al., 2019).

The mixing between fresh groundwater and saline water promotes physicochemical and biogeochemical processes, which depend on the lithological and sedimentological boundary conditions. In addition, the composition of the solution may be further superimposed by diagenetic processes, thereby modifying associated benthic-pelagic element fluxes.

While surface estuaries provide essentially oxygenated waters to the ocean, SGD may also add anoxic waters to the coastal environment (Church, 1996; Moosdorf et al., 2021; Paytan et al., 2006; Santos et al., 2021; Slomp and Van Cappelen, 2004).

Most studies on water and elemental fluxes associated with SGD are derived from the characterization of endmembers (e.g., groundwater, rivers, and surface seawater), with less attention paid to the processes in the mixing zone. However, processes within the subterranean estuary, and particularly in the sediments overlying the aquifers can be impacted by biotic and abiotic transformations, resulting in sources and/or sinks of reactive elements (Böttcher et al., 2024; Charette et al., 2005; Froelich et al., 1979; Goyetche et al., 2022; Huettel et al., 1998; Moore, 1999; Moosdorf et al., 2021; Szymczycha et al., 2023) modifying the composition of the SGD. Ion sorption, mineral dissolution, precipitation, and remineralization of organic matter are among the processes occurring in the aquifers and along the flow path of SGD (Moore, 1999; Moosdorf et al., 2021). In addition, substrate availability, aquifer rock composition, and groundwater residence time are also of great importance. Therefore, the controls on non-conservative behavior must be understood and taken into account when estimating SGD element fluxes to coastal waters (Beck et al., 2007b; Cerdà-Domènech et al., 2017; Donis et al., 2017; von Ahn et al., 2021).

The fresh and saline components of SGD are usually well mixed, making the quantification and its impact on coastal waters complex (e.g. Sadat-Noori et al., 2016). Detection and estimation of SGD have been carried out through various approaches (Böttcher et al., 2024; Burnett et al., 2006; Taniguchi et al., 2019). For example, geophysical techniques identified fluid/gas fluxes across surface sediments (e.g., Hoffmann et al., 2020; Idczak et al., 2020); direct measurements based on piezometers and seepage meters assessed porewater gradients, and quantified SGD and the associated chemical fluxes (e.g., Donis et al., 2017; Oberdorfer et al., 2008; Tamborski et al., 2018).

Among the geochemical tracers, radium, methane, and stable isotopes have been applied in the majority of SGD studies, and the results are promising for detecting, evaluating, and quantifying SGD. For example, water isotopes allowed quantification of mixing processes, as groundwater is depleted in heavier isotopes compared to seawater (Gat, 1996; Povinec et al., 2008). The concentrations and stable carbon isotope composition of DIC, DOC, and CH_4 are powerful tracers to access the biogeochemical processes within the subterranean estuary (Böttcher et al., 2014; Donis et al., 2017; Sadat-Nouri et al., 2016; Winde et al., 2014). Radium is generally more abundant in groundwater than surface water and, therefore, can provide quantitative and qualitative information on the regional occurrence of SGD (Beck et al., 2007a; Moore, 1996, 2006; Moore et al., 2011; Rodellas et al., 2017; Taniguchi et al., 2019; Top et al., 2001; von Ahn et al., 2021).

Studies on SGD have been carried out in the Baltic Sea (e.g., Krall et al., 2017; Peltonen 2002; Purkamo et al., 2022; Purkl and Eisenhauer, 2004; Schlüter et al., 2004; Virtasalo et al., 2019; Viventsowa and Voronow, 2003; von Ahn et al., 2021), particularly in the Gulf of Gdańsk and the Puck Bay, already since the 90s (e.g., Falkowska and Piekarek-Jankowska, 1999; Piekarek-Jankowska, 1996). Dif-

ferent sites of SGD occurrence have been identified throughout the Gulf of Gdańsk and Puck Bay. They act as hot spots for SGD to the surface waters impacting to different degrees the coastal water balance and the biogeochemical cycles within the coastal waters. For example, based on seepage meters, measurement fluxes of SGD and their associated chemical fluxes were estimated for different areas in Puck Bay (Donis et al., 2017; Szymczycha et al., 2012, 2016, 2023). Furthermore, the impact of SGD on the meiofaunal community was investigated by Kotwicki et al. (2014). Donis et al. (2017) evaluated the impact of SGD on the sandy sediments of Hel Bight, Puck Bay. The impact of pharmaceuticals and caffeine via SGD on the Puck Bay surface waters was also evaluated (Szymczycha et al., 2020). A pockmark associated with SGD in the Gulf of Gdańsk was assessed by Idczak et al. (2020). Moreover, a lowered bottom water salinity was observed almost across Puck Bay, indicating an extended impact by SGD (Matciak et al., 2015).

Due to the high number of identified SGD sites along the Polish coast, this area represents a key SGD site in the Baltic Sea. Taking this opportunity, our study in the Gulf of Gdańsk and the Puck Bay evaluated the dynamics of SGD in different lithologies and the importance of the subterranean estuary on the element fluxes associated with SGD. Therefore, the objectives of the present study are 1) to evaluate the impact of SGD on the chemical gradients in surface sediments taking into account the lithology, 2) to estimate the (isotopic) hydrochemical composition of the fresh water component of SGD entering the Puck Bay compared to the possible endmembers (e.g. groundwater and river waters) around Puck Bay, and 3) to estimate the contribution of SGD to the Puck Bay based on local porewater gradients, seepage meters, and for the first time, regionally, using a Ra isotope balance.

The potential physical pathways and indicators of SGD in the central Puck Bay were characterized using acoustic methods. The investigation was further supplemented by a sedimentological and geochemical characterization of sediments under different degrees of SGD impact. Water column and porewater samples were analyzed for major and trace elements, nutrients, sulfide, total alkalinity, dissolved inorganic carbon (DIC), $\delta^{13}C_{DIC}$, methane (CH_4), $\delta^{13}C_{CH4}$, $\delta^{2}H_{CH4}$, $\delta^{2}H_{H2O}$, $\delta^{18}O_{H2O,}$ radium isotopes (^{223}Ra and $^{224}Ra_{ex}$), tritium (^{3}H) and helium (He) isotopes. This multi-method approach highlights the role of SGD in the local and regional water and elemental budgets of the coastal waters of the Baltic Sea. Finally, it provides a basis for future assessments of the hydrological and ecosystem consequences of coastal areas affected by climate change.

2. Methods

2.1. Study area

The Gulf of Gdańsk is located in the southern Baltic Sea (Figure 1). The maximum water depth is about 118 m, and the surface and bottom layer salinity are about 8 and 12, respectively. As the tidal influence is minimal in the southern Baltic Sea, small hydrodynamic of the bay is mainly due to wind and the river plume front of the Vistula River (Dippner et al., 2019). The shallower sediments of the central gulf are covered by clays that, in some places, contain fine-grained sand and silt, whereas the deepest part is dominated by clayey silt (Idczak et al., 2020; Majewski, 1990, Figure 1).

In the eastern part of the Gulf of Gdańsk, the Hel Peninsula forms a semi-enclosed basin called Puck Bay. The bay has a total area of 359.2 km^2 and is divided into two parts: the outer bay, with an average depth of 20.5 m, and the inner bay, a markedly shallower part, called the Puck Lagoon, with an average depth of 3.1 m (Matciak et al., 2011), covering an area of 104 km^2 (Kramarska et al., 1995).

The outer Puck Bay comprises diverse sediments with coarse-grained sands dominating to a depth of about 20 m. Fine sands, silts, silt-clay, and sand-silt-clay are the composition in the deepest parts, and in addition, some sandy beaches, gravel beds, stony outcrops, clay cliffs, and vegetated river mouths are found (see Kłostowska et al. (2019) and references therein, Figure 1). Sediments in the inner part of Puck Bay have a relatively constant grain distribution dominated by fine and medium sands (Figure 1).

Puck Bay is the main drainage area of Cretaceous, Tertiary, and Quaternary aquifers. It affects the direction of the groundwater flow, thereby modeling the groundwater regime of the piezometric groundwater surface. Groundwater flows into the bay occur mainly via seepage through the seabed. The Hel Peninsula also receives groundwater from Holocene aquifers, but these flow directly into the Baltic Sea (see Piekarek-Jankowska (1996) and references therein).

Different areas along the Puck Bay coastline show impact by SGD (e.g., Donis et al., 2017; Kotwicki et al., 2014; Kłostowska et al., 2019; Szymczycha et al., 2012, 2020, 2023), and the present study is both, an initiation and continuation of these studies by applying new approaches. The investigated SGD sites are Hel, Chałupy, Swarzewo, and Osłonino (Figure 1).

2.2. Material and methods

2.2.1. Sampling and sample preparation

The sampling campaigns were carried out in 2009—2011, 2019, and 2021. Fresh groundwater from wells and piezometers, river water, porewater, sediments, and surface water from the Puck Bay, the Gulf of Gdańsk, and the coastal Baltic Sea were sampled (Figure 1). Additional information on the sampling sites is given in Supplementary Table 1.

The outer Puck Bay water column was sampled at 16 sites in June 2009 onboard r/v *Professor Albrecht Penck* (07PE0919) using a conventional CTD and a pump CTD system (Strady et al., 2008) both equipped with a free-flow bottle rosette. In October 2019 surface waters were sampled onboard the r/v *Oceania* at 40 sites (0.5 m), including the central Gulf of Gdańsk and the coastal Baltic Sea, using a pump attached to the vessel. In addition, bottom water was sampled at four sites using Niskin bottles.

Surface water sampling in the inner Puck Bay was done in October 2019 using a rubber boat and in June 2021 using a sailing boat. Water samples were taken via PE syringes and filtered with 0.45 μm cellulose acetate disposable filters (Carl Roth, Karlsruhe, Germany). For Ra isotopes, 100—150 liters of surface water were pumped through a 1 μm

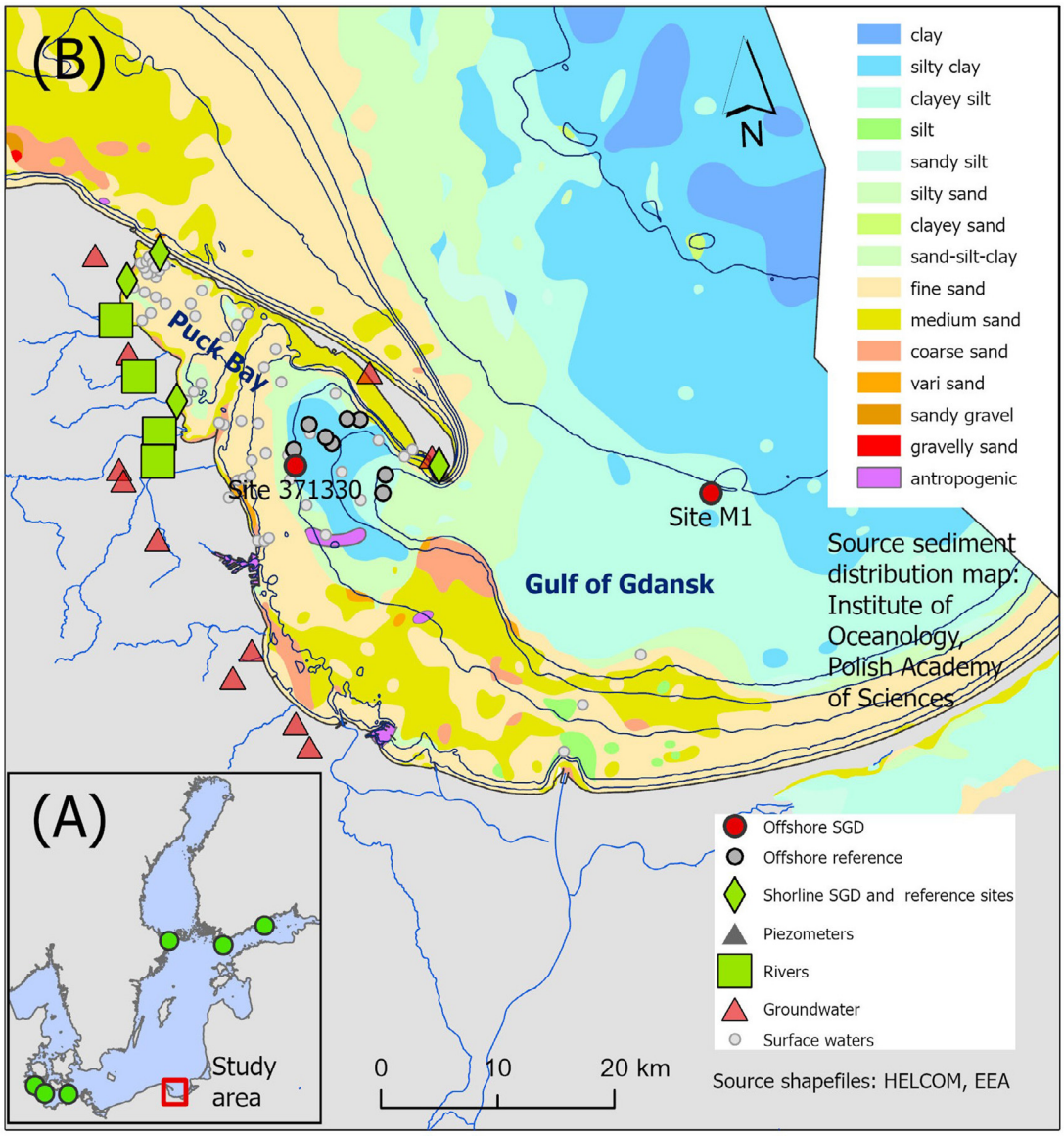

Figure 1 (A) Map showing the location of the study area (red dot) and some of the SGD investigated sites along the Baltic Sea (green dots — Jurasinski et al., 2018; Krall et al., 2017; Purkamo et al., 2022; Racasa et al., 2021; Schlüter et al., 2004; Virtasalo et al., 2019; Viventsova and Voronov, 2003; von Ahn et al., 2021). (B) Map of the study area in the Gulf of Gdańsk/Puck Bay showing the different sampling sites (surface waters, porewater, groundwaters, and rivers). Source of the shapefiles: *European Environmental Agency* (EEA, 2024) *and HELCOM* (HELCOM, 2024) *database*, Atlas of Polish marine area bottom habitats (2009), Environmental valorization of marine habitats (2009) Institute of Oceanology PAS. (The sediment distribution map (modified) was added as a background for a rough overview of the sediment composition of the study area. The map is not georeferenced to the sampled sites.)

filter into barrels. By using a submersible pump, the filtered water from the barrels was pumped through manganese-coated acrylic fibers (Mn-fiber) at a flow rate of around 1 L min^{-1} to quantitatively extract the Ra isotopes. The fibers were washed to remove salt and partially dried for measurements (Garcia-Solsona et al., 2008).

During the cruise in June 2009, sediment cores were retrieved from five sites by a multi-corer device (sites: 371370, 371290, 371330, 37160, 371270), and in October 2019, four sediment cores were retrieved using a GEMAX corer (sites M2, 12M, 15M, 13M) in the outer Puck Bay (Figure 1). In addition, one sediment core was taken in the central Gulf of Gdańsk in 2019 (Site M1). These sites are referred to as offshore sites in this study.

Sediment cores were sliced and frozen for further geochemical analysis. Porewater was extracted from a parallel core via 0.1—0.2 μm rhizons (Rhizosphere Research — Wageningen, The Netherlands; Seeberg-Elverfeldt et al., 2005) and stored in cold or frozen for geochemical analyses. Salinity and pH were measured in situ using a refractometer and handheld pH meter.

Sampling campaigns along the coastline at Hel took place in September and November 2009, March, May, and October 2010, and June 2021. Chałupy, Swarzewo, and Osłonino

were only sampled in June 2021. These sites are referred to as shoreline sites in this study.

Along the shoreline of Puck Bay, porewater was extracted during the campaigns between 2009 and 2011 via pre-established porewater samplers (Donis et al., 2017). During the 2019 and 2021 campaigns, porewater was extracted via push point lances (MHE products) using PE syringes and filtered with 0.45 μm cellulose acetate disposable filters (Carl Roth, Karlsruhe, Germany). For Ra isotopes, 5—10 liters of porewater were transferred into canisters without filtration by a peristaltic pump. From the canister, the sample was filtered through a Mn-fiber as described for the surface water samples from the Puck Bay cruises. Additionally, sediment cores were taken and sliced for further analysis.

Seepage meters were used to measure seepage water fluxes and collect samples for further chemical analysis from sites at Hel, Chałupy, and Swarzewo during the campaign in 2021. The seepage meter consists of a PE chamber with a surface area of 0.7 m^2 connected to a PE bag at the end. The seepage flux rate was calculated from the change in water volume in the bag as a function of time.

Groundwater was sampled in April 2009 and June 2021 from 17 wells and two piezometers at depths varying between 2 and 180 m. Six groundwater wells and two piezometers were located on the peninsula and 11 groundwater wells were located on the mainland. River water samples were collected in April 2011 and June 2021 from the Reda (0.6 km inland from the mouth) the Zagórska Struga (0.1 km inland from the mouth), the Płutnica (0.2 km inland from the mouth), and Gizdepka (0.2 km inland from the mouth). Samples were taken via PE syringe and filtered using 0.45 μm SFCA disposable filters (Carl Roth, Karlsruhe, Germany). For Ra isotopes, 60 L of river water was pumped through a 1 μm filter into barrels, and 20 L of groundwater was transferred without filtration into canisters. The sampled water was filtered from the barrels/canisters through a Mn-fiber as described above.

For the determination of total carbon (TC), total nitrogen (TN), total sulfur (TS), total inorganic carbon (TIC), and total mercury (Hg), sediment aliquots were stored in centrifuge tubes (Sarstedt) and kept frozen until freeze-drying and homogenization using an agate ball mill.

Filtrated water samples for major and trace element analysis were filled into acid-cleaned PE bottles and acidified to 2 vol.% with concentrated HNO_3. Nutrient water samples were filled into pre-cleaned PE bottles. Dissolved sulfide (H_2S) water samples were filled into PE bottles prefilled with ZnAc 5%. Porewater samples for total alkalinity (TA) were collected in PE vials prefilled with 0.1M HCl. Water samples for dissolved inorganic carbon (DIC) and $\delta^{13}C_{DIC}$ were filled without headspace into Exetainer® tubes prefilled with saturated $HgCl_2$ solution. Samples for $\delta^{13}C_{CH4}$ and $\delta^{2}H_{CH4}$ were kept closed in glass containers sealed with a butyl septum (black) and preserved with NaOH solution (Jørgensen et al., 2004). Samples for $\delta^{18}O_{H2O}$ and $\delta^{2}H_{H2O}$ analyses were collected in 1.5 mL glass vials (Zinser) sealed with PTFE-coated septum caps. Samples for ^{3}H were stored in PE bottles. For helium isotopes, samples were allowed to flow through and finally stored in head-space-free copper tubes. All samples were stored in the dark cool, or frozen until further analyses.

The diffuse Ra flux from the bottom sediments of Puck Bay was quantified following the approach outlined by Rodellas et al. (2012), using sediments from the Site Osłonino (Figure 1). The sediments were mainly composed of sand. The sediments were placed in a 3L beaker, and the overlying water was extracted and replaced with Ra-free surface water from Puck Bay (2 L). A closed loop system was assembled, and the water was continuously circulated through the tubing and the Mn-fiber. The Mn-fibers were replaced after 12, 24, 36 and 48 h. The overlying water was constantly aerated to prevent changes in redox conditions. The diffusion rate was calculated from the slope of the accumulated $^{224}Ra_{ex}$ activity (in Bq) per incubation time (h) (Supplementary Figure 2).

2.2.2. Geophysical investigations

High-resolution sub-bottom profiling using an INNOMAR SES96 Standard parametric sediment echo sounder was performed during a cruise with r/v *Professor Albrecht Penck* in 2009. A motion reference unit was used to steer/keep the acoustic beam in the vertical direction to correct the ship's vertical movements. The track plots of the acoustic profiles are shown in Supplementary Figure 1. Detailed descriptions of the SES96 echo sounder system are available at www.innomar.com. During the acoustic survey, the parametric echo sounder transmitted acoustic pulses in a very narrow sound beam with virtually no side lobes and a narrow opening angle of 4 degrees. This resulted in a sonified seafloor area of about 4 m^2 at a water depth of 30 m. The acoustic pulses were built up by a primary frequency component of 100 kHz and a selectable secondary frequency component ranging from 5—15 kHz. Only the secondary low-frequency components penetrated the sub-bottom because the seafloor sediments strongly attenuated the primary high-frequency parts of the acoustic pulses. Depending on the selected secondary frequency, a vertical resolution of sediment layers in the range of 0.2—0.5 m was obtained.

2.2.3. Geochemical analyses

Freeze-dried and homogenized sediments were analyzed for their TC, TN, and TS contents with a CHNS Elemental Analyzer (Eurovector 3000). Combustion was catalyzed by V_2O_5, and the resulting gaseous products were chromatographically separated and quantified via infrared spectrophotometry. Total inorganic carbon (TIC) was determined with an Elemental Analyzer multi-EA (Analytik Jena) after treatment with 40% phosphoric acid followed by infrared spectrophotometric quantification of CO_2. The precision of both methods for the samples from 2019—2021 was about 13, 6, 14, and 6%, and the accuracy was about 2, 12, 8, and 1% for TC, TN, TS, and TIC, respectively, using MBSS- (CNS) and OBSS (TIC) in-house reference materials. The content of TOC was calculated from the difference between TC and TIC. Total mercury (Hg) was analyzed using a DMA-80 (Milestone Microwave Laboratory Systems) analyzer by external calibration with 142R and MBSS reference materials. The detection limit was 0.15 μg kg^{-1} (Leipe et al., 2013) and the precision and accuracy of the measurement for 2019-21 was better than ± 4.5 and ±0.6%, respectively.

In the water samples, the major ions (Na, Mg, Ca, K, S) and trace elements (Ba, Fe, Mn) were analyzed by inductively coupled plasma optical emission spectrometry (ICP-

OES; iCAP 6400 Duo (before 2016), iCAP 7400 Duo, Thermo Fischer Scientific) using matrix-matched external calibration and Sc as internal standard. Precision and accuracy were checked with spiked CASS-4 and SLEW-3 (NRCC) and were better than 4 and 5% for CASS-4, and 7 and 7% for SLEW-3, respectively. In all water samples, the measured total dissolved S is considered to consist mainly of SO_4.

Concentrations of H_2S were determined by the methylene blue method (Cline, 1969) using a Spekord 40 spectrophotometer (Analytik Jena). Nutrients were analyzed using QuAAtro autoanalyzer system (Seal Analytical, Southampton, UK) following Grasshoff et al. (2009).

Total alkalinity (TA) was measured by potentiometric titration (Van den Berg and Rogers, 1987). Dissolved inorganic carbon (DIC) and $\delta^{13}C_{DIC}$ values were determined by means of continuous-flow isotope-ratio mass spectrometry (CF-IRMS) using a Thermo Finnigan MAT253 gas mass spectrometer attached to a Thermo Electron Gas Bench II via a Thermo Electron Conflo IV split interface, as described by Winde et al. (2014). Solutions were allowed to react for at least 18 h at room temperature before introduction into the mass spectrometer. The international NBS19 standard, a carbonate from Solnhofer Platternkalk, and in-house $NaHCO_3$ were used to calibrate measured isotope ratios towards the V-PDB scale. Concentrations of DIC from 2009–2011 were determined based on pH and TA values.

Values of $\delta^{18}O_{H2O}$ and $\delta^{2}H_{H2O}$ were analyzed by a laser cavity-ring-down-spectroscopy (LCRDS) system Picarro L1102-I (2009–2011 data) and Picarro L2140-I (2019–2021 data) (Böttcher and Schmiedinger, 2021; Gupta et al., 2009). Six replicate injections were performed for each sample, and arithmetic averages and standard deviations (1 sigma) were calculated. The reproducibility of the replicate measurements was generally better than 0.7‰ and 0.6‰ (2009–2011 data) and better than 0.06‰ and 0.3‰ (2019–2021 data) for oxygen and hydrogen, respectively. The reference materials SLAP and VSMOW were used to calibrate measured isotope ratios towards the V-SMOW scale. The stable isotope composition of dissolved methane in porewater was carried out at the Centre of Environmental Research (UFZ) (Tamisier et al., 2022). The given '‰' values are equivalent to mUr (Milli Urey; Brand and Coplen, 2012).

^{3}H and He isotopes (^{3}He and ^{4}He) were measured as described by Sültenfuß et al. (2009). Short-lived Ra isotopes (^{223}Ra, $t_{1/2} = 11.4$ d, and ^{224}Ra $t_{1/2} = 3.7$ d) were measured within 3 and 7 days after sampling with a radium-delayed coincidence counter (RaDeCC) (Moore and Arnold, 1996). After about a month, a further measurement was conducted to determine ^{224}Ra supported by ^{228}Th ($t_{1/2} = 1.9$ years). This measurement is then subtracted from the initial ^{224}Ra to obtain the excess of ^{224}Ra activities ($^{224}Ra_{ex}$). The activities of ^{223}Ra, ^{224}Ra, and $^{224}Ra_{ex}$ have been calculated and the expected error of the measurement is 12 and 7% for ^{223}Ra and ^{224}Ra, respectively (Garcia-Solsona et al., 2008). The detectors are calibrated once a month using ^{232}Th with certificate activities.

2.2.4. Flux calculations

Exchange fluxes between sediment and the overlying water were estimated based on measured porewater profiles. To constrain the upward porewater velocity, the salinity gradient formed by mixing fresh groundwater with seawater near the sediment-water interface was fitted. The partial differential equation

$$0 = \frac{d}{dx}\left[\left(\frac{D_m}{\tau^2} + D_e\right)\frac{dC}{dx} - uC\right] \quad (1)$$

describes the concentration profile of sodium, where u is the upward flow velocity, C is the concentration, D_m is the ionic diffusion coefficient, which was corrected for temperature and salinity, $\tau^2 = 1 - 2log\varphi$ is the tortuosity, and φ is the porosity (Boudreau, 1997). The equation does not account for the gradient in porosity, as this would require additional fitting of the porosity while it had almost no impact on the fitted advective velocities. Here, we used D_e to account for additional mixing near the sediment-water interface, which may result from currents and groundwater recirculation (Donis et al., 2017; Qian et al., 2009). This mixing coefficient was the highest value at the sediment-water interface and could be constant in a surficial layer varying between 0 and 7 cm thickness before decaying exponentially over depth.

Our approach was to set D_e to zero when mixing in the top was not apparent and generally used low values, leading to conservative estimates of the upward porewater velocities and submarine groundwater discharge. The bottom-water sodium concentration was used as the upper boundary condition. A zero concentration was imposed as a lower boundary condition. Except in cases where there was no clear gradient at depth signaling the occurrence of SGD, a non-zero concentration was imposed. The equation was solved both numerically with the ReacTran package in R (R Core Team, 2022; Soetaert and Meysman, 2012) and analytically. For the latter, the concentration was assumed to be constant in the upper mixing zone if present, and D_e was set to 0 below. The analytical solution was used to check if the domain depth was sufficiently long so that it did not affect the outcome. The numerical and analytical solutions only differed significantly in cases with weak mixing in the top layer, and then the numerical solution was preferred.

The fluxes of chemicals were estimated by

$$F = -\varphi\frac{D_m}{\tau^2}\frac{dC}{dx} - \varphi D_e\frac{dC}{dx} + \varphi uC \quad (2)$$

where the first, second, and third terms on the right-hand side represent the diffusive, additional mixing, and advective fluxes. Linear regression was used to fit the concentration gradient $\frac{dC}{dx}$ either through points near the sediment-water interface or, in cases with strong mixing at the top, the depth from where a clear gradient was visible. For the porosity, measurements were directly used. The porosity was assumed to be 0.4 for sandy sites, where the porosity had not been measured.

3. Results

An overview of the (isotopic) hydrochemical composition of the surface waters from the open Baltic Sea, surface and porewaters of the Gulf of Gdańsk and Puck Bay, fresh groundwater, and rivers is provided in Table 1.

Table 1 Chemical average, minimum, maximum and, number of samples of the Baltic Sea, Gulf of Gdańsk, outer Puck Bay, inner Puck Bay, rivers, groundwater from wells, groundwater from piezometers, offshore porewaters, shoreline porewaters, the estimated fresh component of SGD, and the seepage meter sample. River results also contain data from Ehlert von Ahn et al. (2023)

Variables	Baltic Sea	Gdańsk Bay	PB outer	PB inner	Rivers	GW_Well Deep	GW piazometer shallow	Offshore SGD impacted PW	Offshore reference PW	Shoreline SGD impacted PW	Shoreline reference PW	Fresh SGD component	Seepage meters
Years	2019	2019	2009 and 2019	2019 and 2021	2011 and 2021	2009 and 2021	2009 to 2021	2009 and 2019	2009 and 2019	2009 to 2021	2009 to 2021	2009 to 2021	2021
Salinity		6.8	6.9	6.8	0.2	0.1	0.3	8	8	3.3	6.4		6.5
		(1)	6.1/7.6 (26)	5.8/7.3 (68)	0.2/0.3 (4)	0.1/0.3 (17)	0.0/0.8 (6)	6/10 (26)	6/9 (83)	0.4/7.2 (103)	5.1-7.3 (27)		5.8/6.9 (4)
pH	8.0	7.8	7.9	8.1	7.7	7.5	7.1	7.3	7.4	7.2	7.3	6.9	7.9
	(1)	7.8 (4)	7.7/8.2 (31)	6.6/8.8 (66)	7.3/8.4 (8)	7.2/8.4 (25)	6.3/7.5 (5)	7.0/7.5 (13)	6.9/7.7 (51)	6.2/8.3 (80)	6.4-8.0 (27)	5.8/8.2 (6)	7.2/8.9 (4)
TA [mM]			1.7						4.9	3.8	2.2	5.1	
			(2)						0.4-15.0 (54)	0.8/7.2 (80)	0.4/7.8 (27)	2.5/7.1 (6)	
DIC [mM]	1.6	1.7	1.6	1.8	4.0		4.6	11	4.7	3.6	2.5	5.7	1.9
	(1)	1.6/1.8 (4)	0.7/1.7 (41)	1.6/2.3 (49)	3.6/4.4 (2)	3.1/9.6 (19)	2.9/6.2 (3)	1.3/24.1 (20)	1.4/13.1 (38)	0.5/8.4 (31)	0.5-7.6 (21)	3.2/8.8 (4)	1.5/2.6 (4)
$\delta^{13}C_{DIC}$ [‰ VPDB]	0	-0.8	-0.5	-0.8	-12.3	-11.8	-20.1	-3.6	-10.4	-9.7	-8.0	-13.6	-8.4
	(1)	-2.5/0.0 (4)	-1.7/-0.1 (32)	-7/0.8 (59)	-13/-11 (2)	-19/-8 (20)	-24/-13 (3)	-14/14 (26)	-18/-1.6 (55)	-26/2.9 (47)	-12/-3.5 (9)	-32.8/-0.6 (5)	-15.5/-5.1 (4)
$\delta^{13}C_{CH4}$ [‰VPDB]										-60			
										-63-(-48) (7)			
$\delta^{2}H_{CH4}$ [‰ VSMOW]										-222			
										-248-(-132) (6)			
$\delta^{18}O_{H2O}$ [‰VSMOW]	-6.4	-6.5	-6.4	-6.3	-9.7	-10.6	-9.6	-6.1	-6.4	-8.7	-6.2	-9.7	-6.7
	(1)	-6.5/-6.4 (4)	-6.7/-6.2 (42)	-7/-5 (53)	-10.2/-9.2 (6)	-13.7/-9.8 (20)	-11.0/-9.1 (6)	-6.6/-5.7 (11)	-6.6/-6.0 (28)	-10.4-(-6.1) (32)	-7.0-5.4 (9)	-10.9/-7.8 (5)	-7.3/-5.8 (4)
$\delta^{2}H_{H2O}$ [‰ VSMOW]	-48.8	-48.7	-48.3	-48.0	-67.2	-74.1	-67.8	-45.8	-48.3	-64.0	-48.3	-69.4	-51.2
	(1)	-49.2/-48.5 (4)	-47.1/-52.6 (42)	-56/-42 (41)	-69.8/-65.3 (6)	-102.2/-66.9 (20)	-80.0/-62.0) (6)	-49.5/-43.1 (11)	-49.2/-47.6 (28)	-76.2-(-47.5) (32)	-51.7-44.0 (9)	-78.4/-56.7 (5)	-54.7/-46.1 (4)
Na [mM]			101	92	0.6	2.3	3.2	107	103	47.2	87.1	3.2	84.4
			84/126 (9)	76/104 (39)	0.2/1.2 (6)	0.2/7.2 (25)	2.8/3.6 (4)	89/135 (26)	87/112 (93)	4-102 (93)	70/103 (24)	0/14 (6)	74/90 (4)
Mg [mM]			11.6	10.7	0.3	0.4	0.3	12.3	11.4	5.2	9.9	0.5	9.9

(*continued on next page*)

Table 1 (*continued*)

Variables	Baltic Sea	Gdańsk Bay	PB outer	PB inner	Rivers	GW_Well Deep	GW piazometer shallow	Offshore SGD impacted PW	Offshore reference PW	Shoreline SGD impacted PW	Shoreline reference PW	Fresh SGD component	Seepage meters
			10.1/13.6 (9)	8.3/11.8 (39)	0.3/0.4 (6)	0.0/0.7 (25)	0.2/0.4 (4)	9.6/16.0 (26)	9.6/13.7 (93)	0.5-11.5 (93)	8.1/11.7 (24)	0/0.9 (6)	8.7/10.3 (4)
Ca [mM]			2.8	2.7	2.0	1.8	2.3	3.1	2.8	2.6	2.9	1.9	2.8
			2.7/3.2 (9)	2.3/3.0 (39)	1.8/2.4 (6)	1.1/3.4 (25)	2.0/2.6 (4)	2.5-3.7 (26)	2.4-3.1 (93)	1.0-8.4 (93)	2.3/4.1(24)	0.7/3.0 (6)	2.7/2.9 (4)
K [mM]			2.1	2.1	0.1	0.1	0.5	2.6	2.4	1.1	1.9	0.4	2.0
			1.8/2.6 (9)	1.6/2.8 (39)	0.0/0.1 (6)	0.0/0.5 (25)	0.4/0.5 (4)	2.1/3.3 (26)	2.0/2.7 (93)	0.2-2.2 (93)	1.3/2.2 (24)	0.1/1.4 (6)	1.8/2.0 (4)
SO_4 [mM]				6.0	0.4	0.7	0.3	3.6	4.2	2.7	4.9	0.1	5.4
				5.1/6.6 (39)	0.3/0.6 (6)	0.0/2.4 (25)	0.2/0.4 (4)	0.2/6.3 (26)	0.3/7.1 (92)	0.0-6.0 (86)	2.6-6.1 (24)	0/0.6 (6)	4.6/5.8 (4)
H_2S [μM]								345	327	87	185		0.5
								0/2041 (26)	0/1683	0-1585 (87)	0-1248 (24)		0/1.0 (4)
Si [mM]			0	0.1	1.1	0.4	0.4	0.5	0.5	0.2	0.1	3.1	0
			(7)	0-0.7 (39)	0.1/1.9 (6)	0.2/0.6 (14)	0.3/0.4 (2)	0.0-0.9 (26)	0.0-0.8 (82)	0/0.6 (44)	0/0.3 (12)	0.2/6.3 (6)	0/0.1 (4)
P [μM]			0.4	1.4	1.6	2.2	43.5	266	112	40	18.0	49.2	3.9
			0.2/1.3 (9)	0.3/9.9 (39)	0.4/3,5 (6)	0.1/5.9 (20)	41.0/46.2 (4)	1.0-668.2 (26)	1.4-310 (93)	0.5/113 (93)	0.6/54.4 (24)	1.8/64.6 (6)	1.5/10.1 (4)
Ba [μM]			0.1	0.1	0.6	0.1	0.2	0.7	0.3	0.1	0.2	0.4	0.2
			0.1/0.2 (9)	0.1-0.2 (39)	0.1/1.3 (6)	0.1/0.7 (25)	0.0/0.5 (4)	0.1-1.7 (26)	0.1-0.5 (93)	0/1.4 (91)	0.1/0.3 (24)	0/2.3 (6)	0.1/0.2 (4)
Fe [μM]			0	0.2	2.2	15	1.5	69	24	48	116	54.8	2.4
			(9)	0/1.3 (39)	1.0/3.9 (6)	0.2/52 (25)	0.1/2.5(4)	0.1-317 (26)	0.0-193 (93)	0/1032(92)	0/795 (24)	0.7/324 (6)	0.4/5.8 (4)
Mn [μM]			0	0.1	1.4	1.8	0.7	8.2	2.6	1.9	1.3	4.2	0.8
			0/0.1 (9)	0.0/0.1 (39)	0.3/3.2 (6)	0.0/4.1 (25)	0.2/1.1 (4)	0.5-21.1 (26)	0-13.5 (93)	0/9.9 (91)	0/6.6 (24)	0.2/15.3 (6)	0.1/2.1 (4)
NH_4 [μM]				0.0	3.7	35	25	1134	200	244	131		7.1
				0.0/0.7 (18)	1.5/5.5 (4)	1.1/170 (15)	15.0/43 (4)	0-4103.0 (25)	53/635 (17)	0/1068 (91)	0.8/974 (27)		1.3/16.2 (4)
^{224}Ra [Bq m^{-3}]	0.3	0.6	0.5	2	0.8	5	21			50			36
	(1)	0.2/1.3 (8)	0.1/0.9 (32)	0.9/10 (28)	0.6/1.2 (4)	0.4/13 (14)	6/49 (3)			10/86 (4)			12/64 (3)
^{223}Ra [Bq m^{-3}]	0	0	0	0	0.1	0.1	1			1.2			1
	(1)	(8)	(30)	0.0/1 (28)	0/0.2 (4)	0/0.4 (13)	0/1 32)			0.5-2.4 (3)			0/2 (2)
$^{224}Ra_{ex}$ [Bq m^{-3}]	0.3	0.5	0.4	2	1	5	20			45			30
	(1)	0.1/1.2 (8)	0.1/0.8 (32)	0.8/10 (24)	0.5/1.0 (4)	0.4/13 (14)	6/48 (3)			10/79 (4)			6/54 (3)

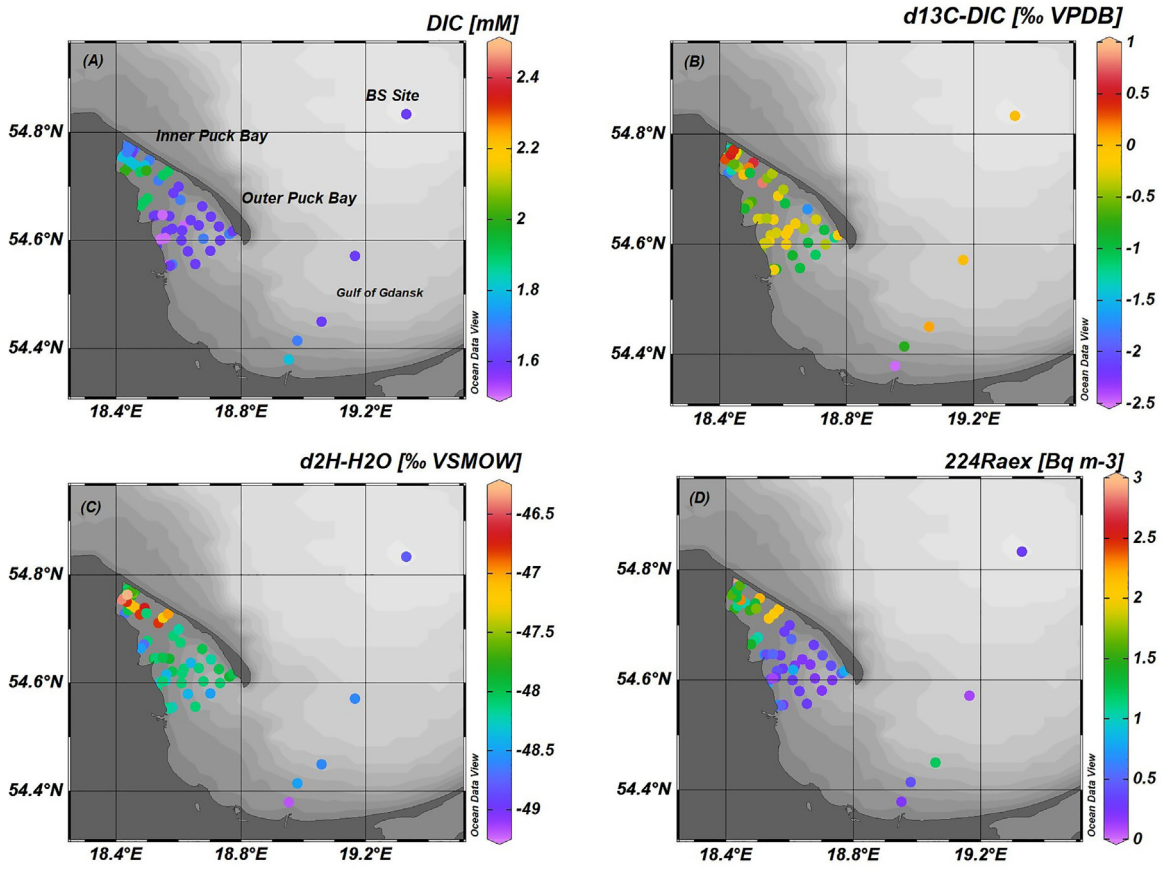

Figure 2 Variation of (A) dissolved inorganic carbon (DIC), (B) δ^{13}C-DIC, (C) δ^{2}H-H_2O, (D) ^{224}Radium-excess. Data of the outer Puck Bay corresponds to the campaign in 2019. Data of the inner Puck Bay correspond to the campaigns in 2019 and 2021. The concentration maps were plotted using Ocean Data View (Schlitzer, 2001). The results from shoreline sites are not presented in the figures.

3.1. Surface water composition

The Puck Bay water isotopic composition varied from −7 to −5‰ and −56 to −42‰ for δ^{18}O and δ^{2}H, respectively (Table 1), with the inner part of the Puck Bay showing heavier values (Figure 2). The samples from the Gulf of Gdańsk and the Baltic Sea revealed a composition in the same range (Table 1).

The DIC concentrations in the Puck Bay surface waters ranged between 0.7 and 2.3 mM, with slightly higher concentrations in the inner part of the bay (Figure 2). The Gulf of Gdańsk and the Baltic Sea showed similar DIC concentrations of about 1.7 mM. The $\delta^{13}C_{DIC}$ signatures ranged from −1.7 to 0.8‰. At sites near the shoreline where SGD has been observed, the signatures reached −6‰. The Gulf of Gdańsk showed $\delta^{13}C_{DIC}$ values between −2.4 and 0.1‰, with the isotopically lightest value being close to the coastline and probably affected by the Vistula River discharge (Figure 2). The Baltic Sea Site had a carbon isotopic signature of DIC of about 0‰ during sampling.

The $^{224}Ra_{ex}$ activities in the surface waters varied between 0.1 and 3 Bq m^{-3} (Table 1, Figure 2). The average activities in the Baltic Sea, Gulf of Gdańsk, and outer Puck Bay were 0.2, 0.5, and 0.4 Bq m^{-3}, respectively, while the inner part showed a much higher level up to 3 Bq m^{-3}. Activities of ^{223}Ra showed similar behavior to $^{224}Ra_{ex,}$ with values ranging between near 0 and 0.2 Bq m^{-3} (Table 1).

Bottom water $^{224}Ra_{ex}$ activities measured at three sites in the outer Puck Bay showed slightly higher values of 0.3, 0.3, and 0.6 Bq m^{-3} than the surface water activities of 0.2, 0.2, and 0.4 Bq m$^{-3,}$ respectively. In contrast, a more distinct difference appeared in the Gulf of Gdańsk, where bottom and surface water $^{224}Ra_{ex}$ activities were 4 and 0.1 Bq m$^{-3,}$ respectively.

The investigated shoreline sites Hel, Chałupy, Swarzewo, and Osłonino (Figures 1 and 2) revealed particularly high Ra activities in surface waters with activities of $^{224}Ra_{ex}$ of 2, 9, 9, and 3 Bq m^{-3}, and ^{223}Ra activities were 0.1, 0.3, 0.5, and 0 Bq m^{-3}, respectively.

3.2. Geophysical characterization of sediments of the outer Puck Bay

Acoustic sub-bottom images from the muddy central part of the outer Puck Bay are displayed in Figure 3. In both images, the sea bottom echo is weak, indicating a low contrast in acoustic impedance between the water and bottom sediments, a typical feature for soft mud sediments. The thickness of this nearly acoustic transparent mud layer is about 1 m in the central part of the bay and thins out towards the SE slope of the basin. Moreover, it is possible to observe that

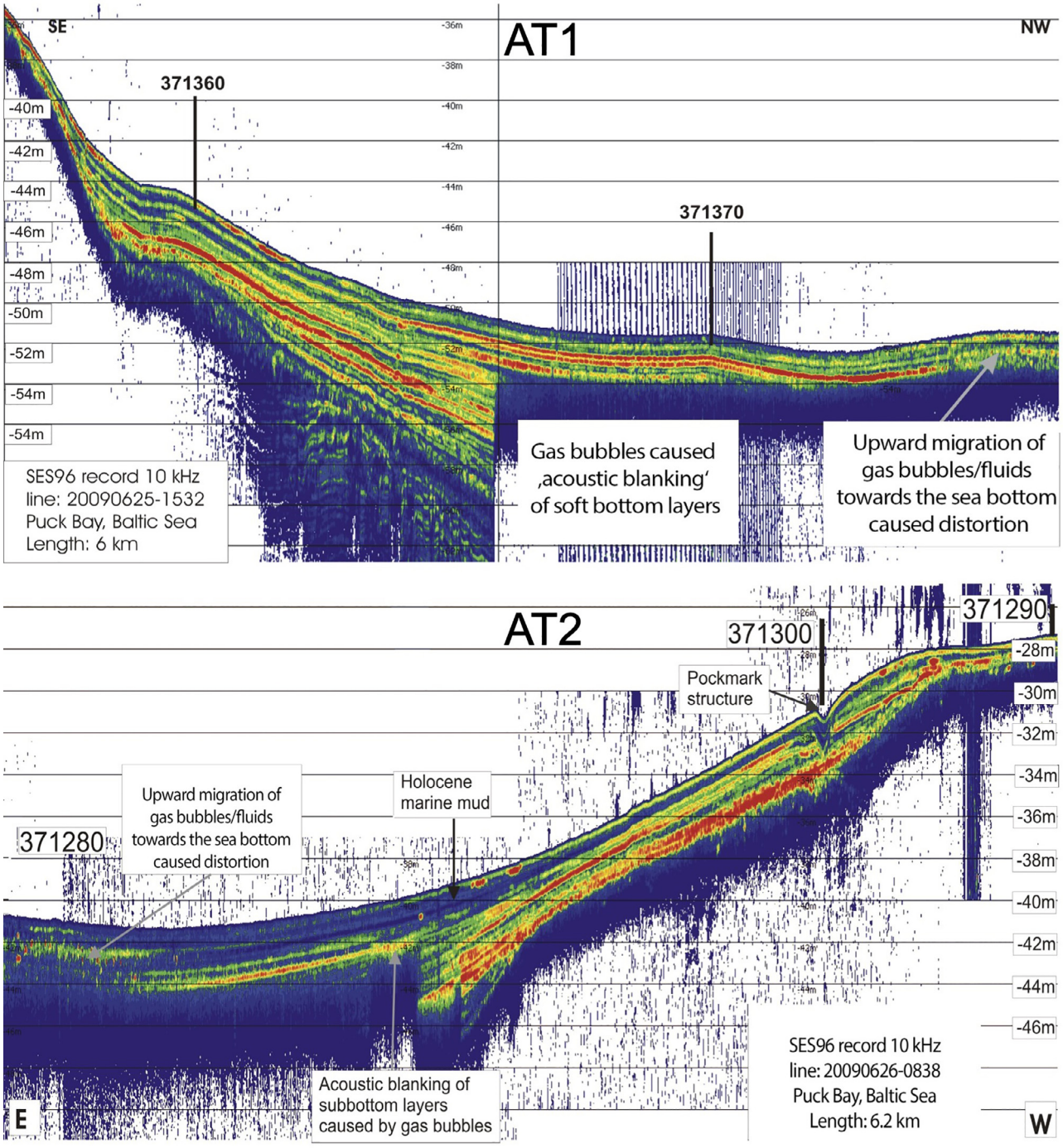

Figure 3 Acoustic transects AT1 and AT2 modified from Böttcher et al. (2024) from the Outer Puck Bay from the campaign in 2009.

the deposits below are well-stratified and reflect the different stages of the Holocene's marine, brackish, and limnic periods. Some of the deepest reflections may originate from late Pleistocene deposits.

The well-stratified sub-bottom images of both transects are suddenly interrupted in the center of the bay at a depth of about 2.5 m below the seafloor. This is caused by tiny gas bubbles present in the pore space of the sediments. Depending on the frequency-gas bubble size ratio, these bubbly layers can act as an acoustic shield, thereby, absorbing, scattering acoustic energy, and hiding deeper structures. Gas bubbles (mainly CH_4) may originate from the decomposition of organic matter in the underlying sediments. The absence of gas bubbles in the uppermost sediments is likely caused by anaerobic CH_4 oxidation (Iversen and Jørgensen, 1985; Whiticar and Faber, 1986).

Towards the NW end of the transect (Figure 3B), the acoustic image of the uppermost mud layer changes to a

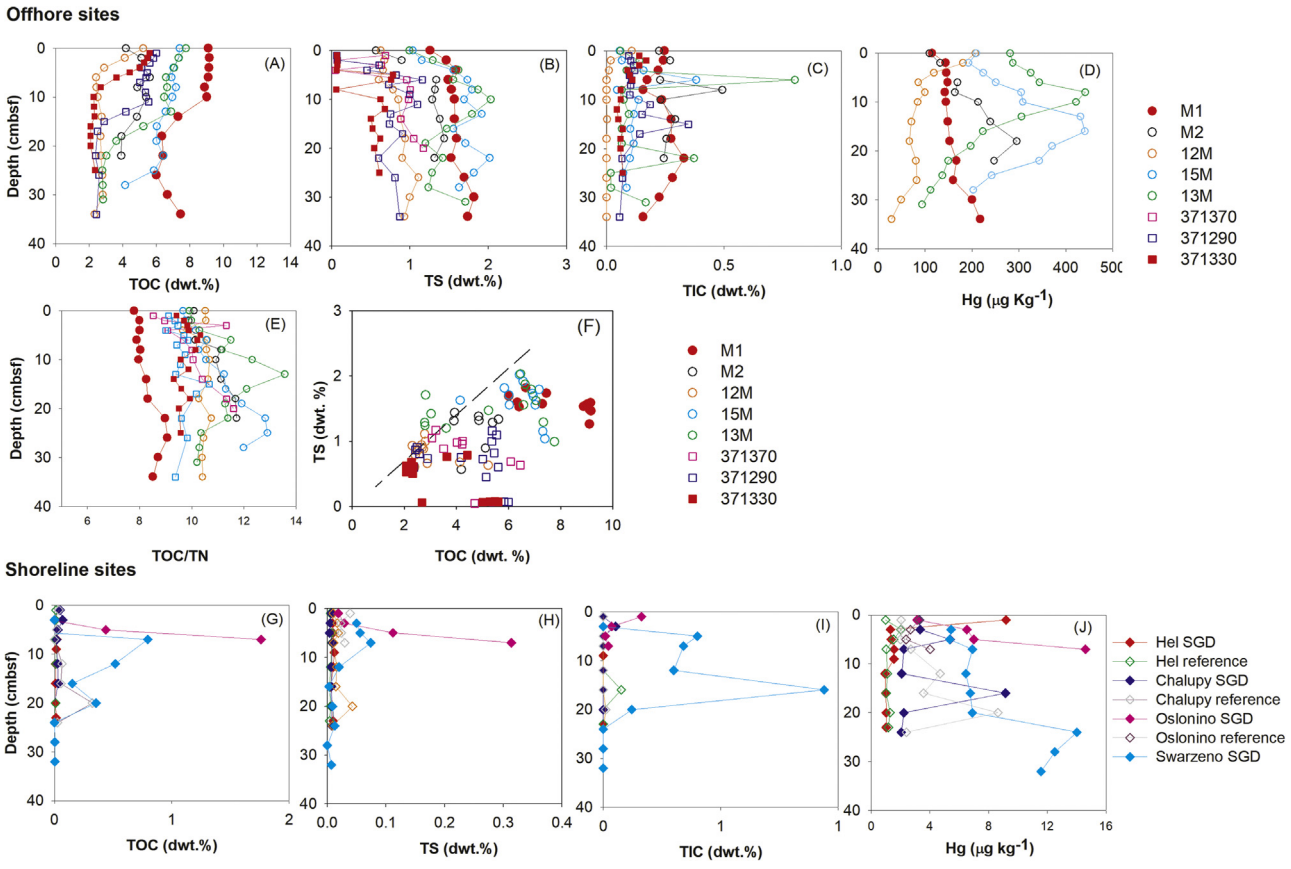

Figure 4 Vertical profiles of bulk geochemical parameters in the sediments from muddy sites (A—F), data from 2009—2019, and sandy sites (G—J) from 2021. Sediment profiles of TOC/TN at the muddy sites (A). Dashed line marks in panel F mean the relationship suggested for Holocene siliciclastic sediments (Berner, 1982). Note: The original definition of (B), (F), and (H) are based on the reducible sulfur (TRIS) content.

more diffuse appearance. This might indicate additional diffusive fluid flow from deeper sources toward the sea bottom, transporting small amounts of gas bubbles. These gas bubbles act as acoustic scatters, masking the sedimentary structure. Moreover, related diagenetic changes of the solid phase, e.g., by precipitation, may produce dispersive distributed acoustic scatters.

Although pockmarks were found, there were no indications of gas bubbles in the sediment or in the water column. Fluid flow along permeable, fractured zones in the sub-bottom may cause these pockmark structures.

3.3. Sediment geochemistry

The site in the Gulf of Gdańsk (Site M1) had the highest TOC content reaching 9% dwt in the top sediments. The content of TOC at the sites of the outer Puck Bay ranged from 2 to 8% dwt, with values decreasing with depth (Figure 4A). In contrast, the surface sediments from the sandy sites at the shoreline were characterized by distinctly lower TOC contents (< 1% dwt., Figure 4G), except for one site located in the inner part of the bay (Osłonino), which showed a maximum of 2% dwt. at 7 cmbsf.

Along with the TOC content, the molar TOC/TN ratio ranged between 8 and 10 at Site M1 (Figure 4E), indicating a dominant proportion of marine organic matter. The sites at the outer Puck Bay showed values between 8 and 13.

Contents of TS at the site in the Gulf of Gdańsk and the outer bay sites varied between near zero and 2% dwt. without apparent differences between the sites (Figure 4B). The accumulation of sedimentary TS indicates the activity of dissimilatory sulfate reduction and deposition of authigenic sulfides. TS further displayed a positive correlation with the TOC content, typical of brackish marine sediments that are limited by the availability of organic matter (Berner and Raiswell, 1983) (Figure 4F). Most of the surface sediments contained calcium carbonate, likely biogenic shell remains, as indicated by the vertical TIC profiles (Figure 4C) that could interact with pore fluids to build up alkalinity.

Vertical profiles of Hg content (Figure 4D) partially indicate the zone of surface sediments deposited during times of high anthropogenic impact (Leipe et al., 2013). However, some profiles are superimposed by physical disturbance such as sediment resuspension, ripple movement, and bioturbation (e.g., Huettel et al., 1998). Pronounced differences in the shape of Hg gradients and absolute contents at several sites suggest different exposures and sediment reworking. While Site M1 showed constant Hg values at depth and some sites even intense mixing down to the observation depth, three sites in the more protected outer Puck Bay displayed

Hg maxima in the top 10 to 20 cmbsf, other sites showed intense mixing down to the observation depth. Different from the offshore sites, the shoreline sandy sites did not exceed Hg contents of 15 $\mu g\ kg^{-1}$ due to the low abundance of substrate for Hg fixation (organic matter and metal sulfides) and strong dilution by quartz.

3.4. Porewater geochemistry

The porewater profile from Site M1, in the Gulf of Gdańsk, showed a decrease in salinity from 10 at the top to 8 at the bottom. The region where Site M1 is situated is already known for gas, and freshwater upflow (Idczak et al., 2020). The porewater salinity of the majority of the sites in the outer Puck Bay displayed values between 6 and 9 and an increase with depth (Figure 5A). In contrast, the salinity at Site 371330 also located in the outer Puck Bay decreased from 7.3 to 6.4.

At the sandy shoreline sites, all sampled porewater profiles showed some freshening at depth, indicating a substantial influence of fresh groundwater at the shoreline of Puck Bay (Figure 6A). Therefore, porewater profiles with at least a 70% decrease in salinity at depth are considered, in this study, as SGD-impacted sites, whereas all others are used as reference sites. The salinity in the reference profiles ranged from 7.3 to 5.1, and at the SGD-impacted sites, salinity even dropped to 0 at depth. Conservative ions such as Na, K, and Mg followed the salinity trends in all profiles.

The $\delta^{18}O_{H2O}$ and $\delta^{2}H_{H2O}$ isotope compositions at the outer Puck Bay sites ranged from −6.6 to −6.0‰ and −49.2 to −47.6‰ respectively. At Site M1 values decreased from −5.7‰ at the sediment-water interface to −6.6‰ at depth and from −43.1 to −49.5‰, respectively. At the reference sites from the shoreline, $\delta^{18}O_{H2O}$ and $\delta^{2}H_{H2O}$ signatures varied from −7.0 to −5.4 and −51.7 to −44.0‰ respectively, whereas at the SGD-impacted sites, the values showed a substantial difference throughout the profile. There, the signatures ranged between −10.4 and −6.1‰ and −76.2 and −47.5‰ for $\delta^{18}O_{H2O}$ and $\delta^{2}H_{H2O,}$ respectively. In addition, analyses of ^{3}H showed higher values in the porewaters of the SGD-impacted sites compared to the bottom waters of Puck Bay (Supplementary Table 2).

Values of pH increased with depth at the offshore sites. Conversely, the pH values at the sandy sites showed a typical decrease with depth from 8.3 to 6.2 (Figure 6E). Concentrations of DIC at the Puck Bay sites, including Site 371330, ranged between 2.0 and 13 mM, whereas Site M1 showed higher concentrations of up to 25 mM in the deeper sediments (Figure 5E). The $\delta^{13}C_{DIC}$ signatures decreased with depth at most sites. However, there were two sites where the $\delta^{13}C_{DIC}$ signatures became heavier with depth, especially at Site M1 showing values up to +13‰ (Figure 5F). Concentrations of DIC at the shoreline sites ranged between 0.5 and 8.4 mM, with the SGD-impacted sites showing higher concentrations (Figure 6F). Signatures of $\delta^{13}C_{DIC}$ were between −11.9 and −3.5‰ at the reference sites on the shoreline. The SGD-impacted sites displayed considerable variability with values ranging between −25.9 and +2.9‰.

At the sandy site on the Hel Peninsula, SGD was associated with CH_4 contributed from the fresh water component (Donis et al., 2017). The stable C and H isotopic composition of CH_4 was measured in 2010 and was found to be isotopically light with stable isotope values varying from −63 to −60‰ and −248 to 240‰ for $\delta^{13}C_{CH4}$ and $\delta^{2}H_{CH4}$ respectively (Table 1). However, a sample close to the sediment-water interface showed a heavier isotopic composition of −48‰ for $\delta^{13}C_{CH4}$ and −132‰ for $\delta^{2}H_{CH4}$ than those taken from deeper sediment sections (Supplementary Figure 4).

Concentrations of SO_4 at the offshore sites ranged between 0.1 and 6.4 mM, decreasing with depth. Some of the sites already had values close to 0 at 20 cmbsf. At Site 371330, a less pronounced decrease in the SO_4 concentrations was found, dropping from 6.1 to 2.6 mM at depth. Site M1 showed lower SO_4 values already at the sediment-water interface compared to the bottom waters, and SO_4 was consumed at a depth of about 15 cmbsf. Most sites showed the typical decrease in SO_4 and an increase in H_2S with depth, with concentrations of the latter ranging between 0 and 1683 μM. In contrast, Site 371330 showed no accumulation of H_2S along the entire profile. Site M1 showed a decrease in H_2S concentrations with depth, with values higher than 2000 μM in the top sediments. At all sandy sites, rapid depletion of SO_4 from bottom water concentrations of around 6 mM down to values below the detection limit was observed. Mixing with fresh groundwater seems to be the dominant factor for very low SO_4 concentrations already at 10 cmbsf at the SGD-impacted sites. In contrast, the SO_4 ranged from 6.1 to 2.6 mM at the reference sites. The sandy shoreline sites did not show any accumulation of H_2S, except for Site Chałupy, which showed values up to 1500 μM at depth.

Without showing clear vertical gradients, concentrations of dissolved Ba ranged between 0.1 and 0.5 μM at all sites in Puck Bay. Site M1 reached values up to 1.7 μM (Figure 5J). The sandy sites displayed spatial variation with higher concentrations found in Osłonino and Swarzewo, where values reached up to 1.4 μM. In contrast, all values were below 0.5 μM at the Hel site. In agreement with an assumption that the solubility of BaSO4 may lead to a reversed concentration behavior, the trends in dissolved trace Ba tend to show the opposite trend and increase with depth. A comparison between Site M1 and the other ones from the central Puck Bay make clear that also the processes or reservoir sizes for metal sources in the fluids differ.

With maximum values in the top sediment, dissolved Fe concentrations varied between near zero levels and 192 μM for most offshore sites. Site 371330 showed the same trend, but the values in the top sediments reached up to 317 μM (Figure 5J). Site M1 showed concentrations close to the detection limit over the entire core depth. Similar to Fe, concentrations of Mn were higher in the top sediments reaching a maximum of 14 μM, with the Site 371330 showing the highest values (Figure 5L). Dissolved Fe revealed very heterogeneous profiles among the shoreline sites, ranging between near zero and 1032 μM. There was no difference between SGD-impacted and reference sites; however, the concentrations showed a high temporal variability at the Hel site. For example, samples collected in 2009 showed maximum Fe concentrations of only 27 μM, whereas the values exceeded 1000 μM in 2010. At the sandy sites, the concentrations of Mn showed a pronounced variability, as observed for Fe. There, the Mn concentrations ranged between near zero and 10 μM. The highest Mn levels were observed at Swarzewo

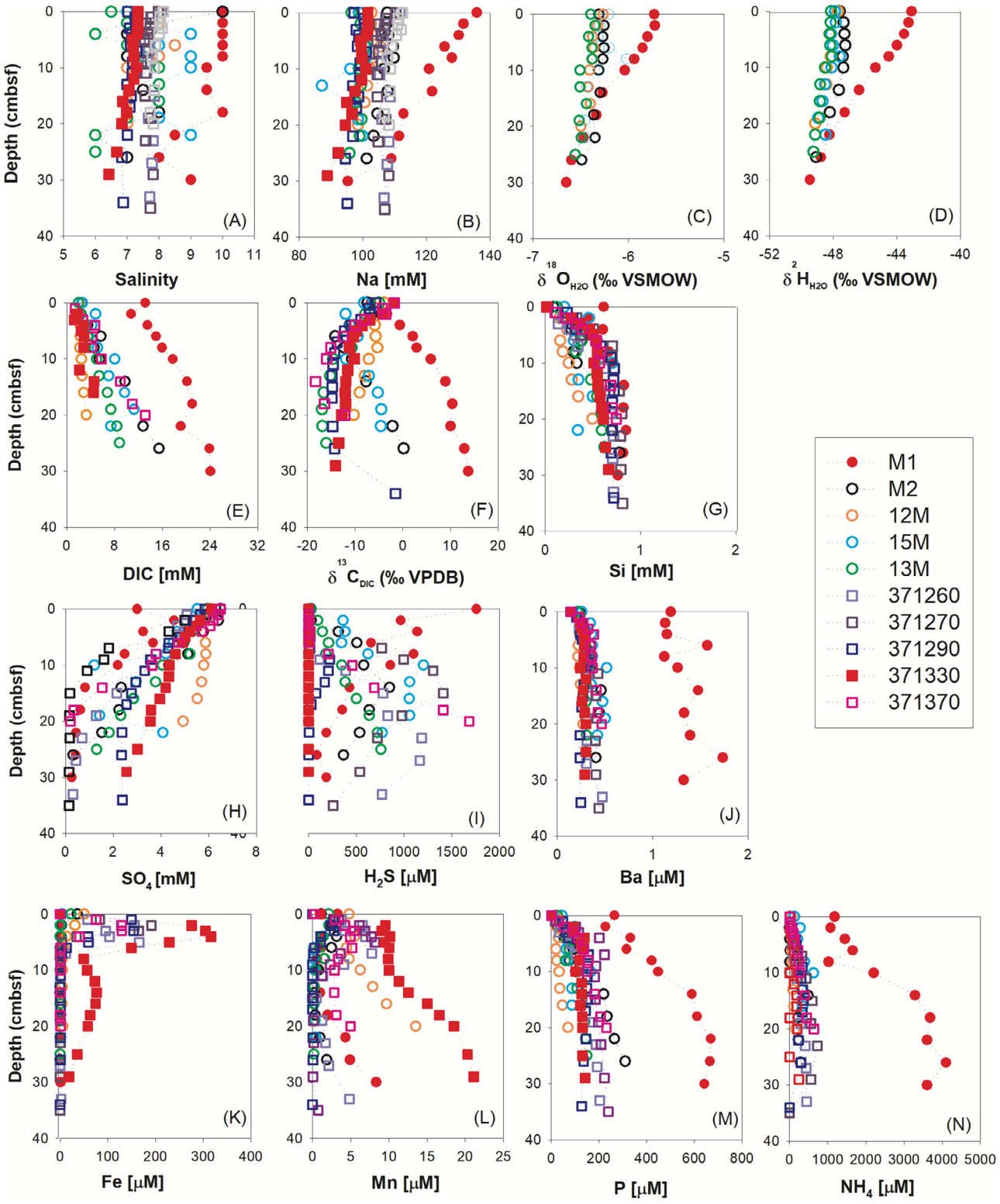

Figure 5 Porewater gradients of geochemical parameters in sediment cores from the muddy sites in Puck Bay and one in the Gdańsk Bay (Gdańsk SGD). Samples from 2009 are represented by circles and from 2019 by squares. Filled symbols refer to SGD-impacted sites.

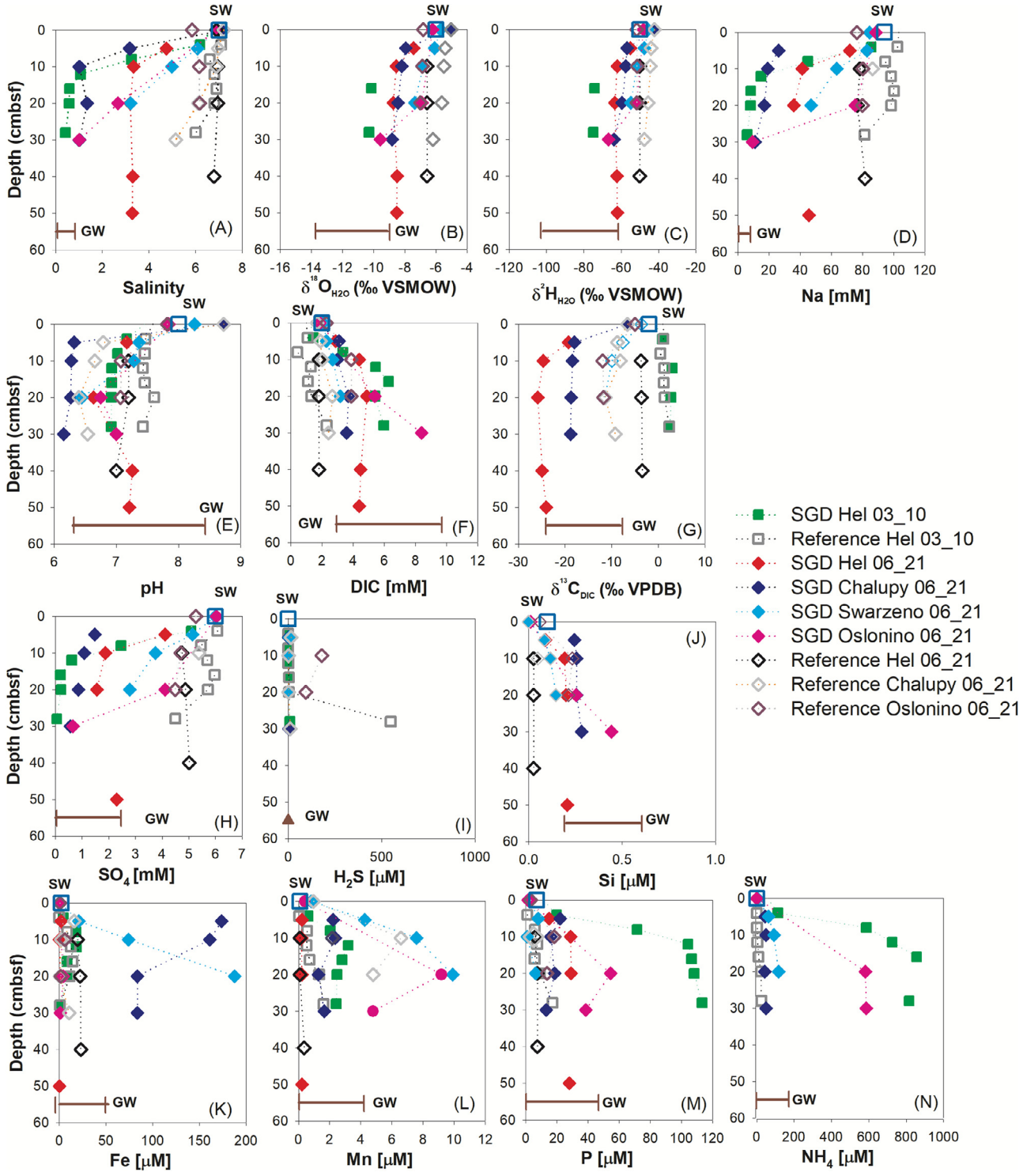

Figure 6 Porewater profiles from the selected sandy site from Hel, Chałupy, Swarzewo, and Osłonino in Puck Bay. Filled symbols represent SGD-impacted sites. All porewater profiles collected from 2009 to 2021 are presented in Supplementary Figure 3.

and Osłonino, and the Hel site again showed higher concentrations in 2010.

Regarding the nutrients, Si concentrations were between near zero and 0.8 mM, with only minor differences between the offshore muddy sites. In contrast, the shoreline sites revealed a difference between the reference and SGD-impacted sites (Figure 6J). While Si increased up to 0.3 mM at the reference sites, twice as high a concentration of 0.6 mM was reached at the SGD sites. Concentrations of P ranged between 0.1 and 240 µM and increased with depth at all offshore sites. Site M1 showed the highest concentration up to 668 µM at depth. Concentrations of P also increased with depth at the sandy sites. The SGD-impacted sites showed a maximum value of 113 µM, whereas the con-

centrations at the reference site remained below 60 μM. Concentrations of NH_4 ranged between 1.4 and 724 μM at the offshore sites in Puck Bay, with Site M1 again showing the highest value (4103 μM) with depth. At the shoreline sites, concentrations of NH_4 were higher at the SGD-impacted sites showing values increasing from near zero at the sediment-water interface to 1068 μM at depth. The reference sites reached a maximum value of 146 μM at a depth of 30 cmbsf.

Activities of $^{224}Ra_{ex}$ were measured in the porewaters at the shoreline sites at a depth of around 50 cmbsf, and the values were 37, 54, 79 and 10 Bq m^{-3} for Hel, Chałupy, Swarzewo, and Osłonino, respectively.

3.5. Direct measurement of seepage rate

Seepage meters were applied in Hel, Chałupy, and Swarzewo (Figure 1) to measure the volumetric seepage rates during the campaign in 2021. These measurements determined the total water flux, but not necessarily the freshwater discharge. However, lowered salinity and water isotopic values demonstrate at least the presence of a freshwater compound.

At the Hel site, the water volume change in the seepage meter bags over time intervals of 85 and 120 minutes equaled a seepage rate of 45 and 30 L m^{-2} d^{-1} respectively. The amount of water collected at the Chałupy Site over 143 minutes yielded a seepage rate of 3 L m^{-2} d^{-1}. At the Swarzewo Site, a flux of 1.6 L m^{-2} d^{-1} was obtained over 170 minutes.

The salinity of the samples collected at Hel was 5.7 and 6.6, and the corresponding surface water salinity was 6.9. The isotopic composition of the water was lighter than the surface water of Puck Bay (Table 1, Figure 6), reaching values for $\delta^{18}O_{H2O}$ of −7.1 and −6.6‰ and $\delta^{2}H_{H2O}$ of −53.4 and 50.8‰. At Chałupy Site, the salinity of the seepage water (6.9) was only marginally lower than that of surface water (7.2). The water isotopic signature revealed $\delta^{18}O_{H2O}$ values of −7.3‰ and $\delta^{2}H_{H2O}$ of −54.7‰. At Site Swarzewo, the salinity was 6.6 in the seepage water and 6.9 in the surface water. The water isotopic signature was relatively light in the seepage water compared to the surface water (Table 1), with values of −5.8 and −46.1‰ for $\delta^{18}O_{H2O}$ and $\delta^{2}H_{H2O}$ respectively.

The fresh groundwater fraction for each site was calculated by assuming that the sample collected in the seepage bag is a mixture of groundwater and recirculated seawater and by applying an end-member model as:

$$V_s \times S_S = V_{gw} \times S_{gw} + V_{sw} \times S_{sw} \quad (3)$$

where *S* and *V* are salinity and volume, the subscripts *S*, *G*, and *SW* represent the sample, groundwater, and seawater fractions, respectively.

The fresh groundwater fractions at the Site Hel were 4 and 17%, corresponding to fresh groundwater fluxes of 0.05 and 0.5 L m^{-2} d^{-1}. For site Chałupy, a fraction of 4% freshwater was estimated, which corresponds to a flux of 0.01 L m^{-2} d^{-1}. At Site Swarzeno, the fresh fraction was 3%, and a fresh groundwater flux of 0.004 L m^{-2} d^{-1} was obtained.

3.6. Coastal groundwater and surface water entering the Puck Bay

3.6.1. Groundwaters

The groundwater comprises the water sampled from wells (deep groundwater) and piezometers (shallow groundwater) around the coastal zone of Puck Bay. A summary of the measured parameters is presented in Table 1.

The groundwater isotopic composition of the deep groundwaters varied from −13.7 to −9.8‰ and −102.2 to −66.9‰, whereas the groundwater at the piezometers ranged from −11.0 to −9.1‰ and −80.0 to −62.0‰ for $\delta^{18}O_{H2O}$ and $\delta^{2}H_{H2O,}$ respectively (Table 1, Figure 7). The measured isotopic signatures from the groundwater wells represent groundwater coming from the Cretaceous, Tertiary, and Quaternary deposit based on Piekarek—Jankowska (1996). In contrast, the heavier signatures of the shallow groundwaters were influenced by meteoric water.

^{3}H values were highest in the shallow groundwater flowing within the Quaternary strata. Very low activity was found in the groundwaters from the Tertiary and Cretaceous aquifers (Supplementary Table 2). A combined evaluation of ^{3}H and He isotope analyses indicates ages of about 30, 50—100, 28, > 60, and >>>60 years for wells Wladyslawowo 2, Reda IV (low ^{3}H, but no ^{4}He), Reda 12c, Rumia (low ^{3}H, but low ^{4}He), and the deep production well on Hel Island (low ^{3}H, but high ^{4}He), respectively (Supplementary Table 2). ^{3}H free older water appears to be further mixed into the Wladyslawowo 2 groundwater.

The hydrogeochemical groundwater composition for most deep and shallow groundwaters is classified as Ca-Mg-HCO_3 type (Figure 7B). Some groundwaters contain higher Na contents, indicating a mixed type. According to Löffler et al. (2010), this water can be further classified as “old groundwater”. Groundwater coming from Cretaceous aquifers was classified as HCO_3-Na according to Piekarek-Jankowska (1996).

Concentrations of DIC were between 3.1 and 6.2 mM, except in Chałupy, where the piezometer sample revealed a value of 2.9 and 9.0 mM in the groundwater well. The $\delta^{13}C_{DIC}$ signatures were spatially heterogeneous. The shallow groundwater showed $\delta^{13}C_{DIC}$ values ranging between -23.8 and −12.1 ‰, with lighter signatures at Hel Site. Signatures in the deeper groundwaters ranged between −12.5 and −8.1‰. Heavier values in deeper groundwaters might be associated with the interaction with carbonates, and less contact with organic matter is expected in confined aquifers. Calcium concentrations were higher in the shallow groundwater, with an average concentration of 2.3 mM, whereas the deep groundwater had an average concentration of 1.8 mM.

Activities of $^{224}Ra_{ex}$ in the deep groundwater ranged between 0.3 and 13 Bq m^{-3}, and the ^{223}Ra activities ranged between 0 and 0.4 Bq m^{-3}. The $^{224}Ra_{ex}$ activities in the groundwater from the piezometers at the Hel site were 7 and 4 Bq m^{-3} for the campaigns in 2019 and 2021, respectively. The piezometer in Chałupy showed higher $^{224}Ra_{ex}$ activities of 48 Bq m^{-3} in 2019. Activities of ^{223}Ra were 0.2 and 1 Bq m^{-3} for Hel and Chałupy during the campaign in 2019.

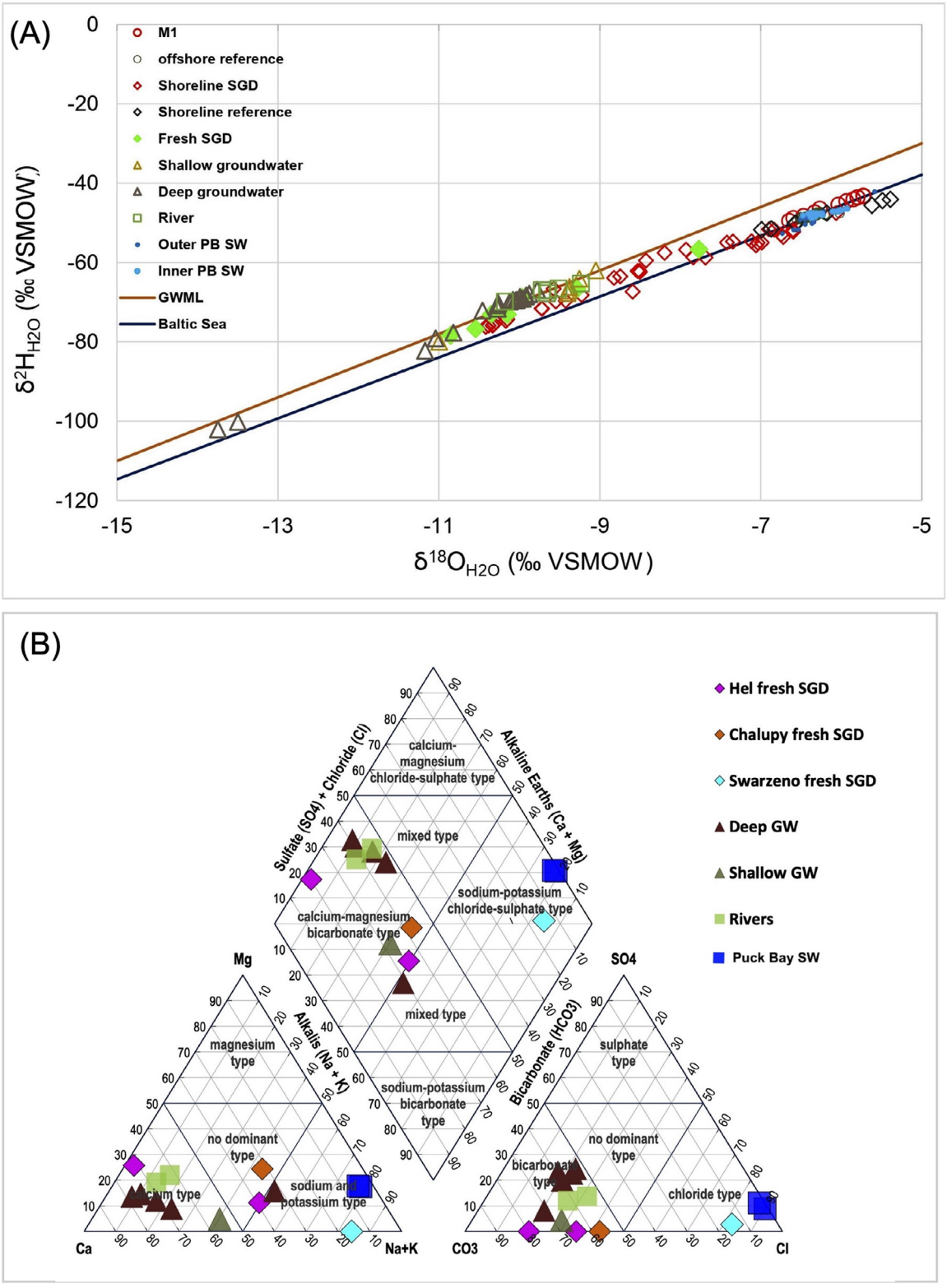

Figure 7 (A) The covariation of $\delta^{18}O_{H2O}$ and $\delta^{2}H_{H2O}$ of sandy sites impacted and non-impacted by SGD, muddy sites impacted and non-impacted by SGD, groundwaters, rivers, and Puck Bay surface water. The global meteoric water line (GMWL), and the Baltic Sea line (Böttcher et al., unpublished data.) are given for comparison. (B) Piper diagram of the major ions of the rivers (green square), deep groundwater (brown triangle), shallow groundwater (dark green triangle), extrapolated porewater from the SGD impacted sites (pink and orange diamond), and porewater. (Graph created from Stosch, 2022).

3.6.2. Rivers

The sampled rivers draining into Puck Bay were Reda, Płutnica, Zagórska Struga, and Gizdepka. A summary of the results is presented in Table 1.

The rivers showed water isotope signatures ranging from −10.2 to −9.7‰ and −69.8 to −67.0‰ for $\delta^{18}O_{H2O}$ and $\delta^{2}H_{H2O}$ respectively. The hydrogeochemical composition of the rivers is classified as Ca-Mg-HCO_3, similar to most groundwaters (Figure 7B).

Average DIC and $\delta^{13}C_{DIC}$ values were 4.0 mM and −12.3‰, respectively. Concentrations of Ca ranged between 1.8 and 2.4 mM.

The Ra activities in the river samples exhibited a small variability with average $^{224}Ra_{ex}$ and ^{223}Ra activities of 1.1 Bq m^{-3} and 0.1 Bq m^{-3}, respectively.

4. Discussion

4.1. Submarine groundwater discharge in the Gulf of Gdańsk and Puck Bay

The bottom waters of Site M1 located in the Gulf of Gdańsk were characterized by high $^{224}Ra_{ex}$ activities compared to the surface waters, indicating the occurrence of SGD, as Ra is mainly derived from groundwater (Beck et al., 2007b; Moore, 2000a; Rodellas et al., 2012). Furthermore, at this site, the sediment porewater showed a decrease in salinity and water isotope signatures at depth (Figure 5A), which could be caused by an upward flux of fresh groundwater. This finding is in line with previous investigations conducted in the region of Site M1, where upward flows of freshwater and gas coming from a pockmark structure were reported (Brodecka-Goluch et al., 2022; Idczak et al., 2020).

The outer part of Puck Bay revealed also higher $^{224}Ra_{ex}$ activities in the bottom water when compared to the surface water at some sites. In addition, acoustic images revealed sediment layers with a pronounced diffuse appearance (Figure 3) than what would be expected only from CH_4 bubble formations, indicating an additional flow. In these images, pockmark structures are also visible. Pockmarks are craters on the seabed that are considered to result from fluid flow (Hovland et al., 1987), including groundwater discharge. It is worth mentioning that pockmarks associated with SGD have been found in many places around the Baltic Sea, for example, in Eckernförde Bay (Germany), Hanko Bay (Finland) and the Gulf of Gdańsk (Hoffman et al., 2020; Idczak et al., 2020; Purkamo et al., 2022; Virtasalo et al., 2019; Whiticar and Werner, 1981). Therefore, it can be inferred that SGD is not just limited to specific spots, but can also occur in multiple areas throughout the bay.

In the outer Puck Bay, the Site 371330 showed a decrease in the porewater salinity with depth, thus considered to be an SGD spot in the central outer Puck Bay.

When comparing the two parts of Puck Bay, submarine groundwater discharge was more evident in the surface water of the inner part of the bay than in the outer part, particularly when pointing out the Ra activities, which showed a more than 4-fold enrichment compared to the activities determined in the more open coastal Baltic Sea. This is partly due to the lower water depths, which allow a stronger signal from mixing with freshwaters and less volume for dilution. In addition to Ra activities, the stable isotope tracers revealed a contribution from different water masses to this area. For example, $\delta^{2}H_{H2O}$ and $\delta^{13}C_{DIC}$ showed high spatial variability, with some areas presenting lighter isotopic signatures (Figure 2) potentially contributed by porewater and/or groundwaters. Concentrations of DIC were slightly higher in the inner bay (Figure 2), indicating impact by porewater fluxes.

Besides the offshore SGD sites (sites M1 and 371330), the shoreline of Puck Bay is also known for several SGD spots (e.g., Donis et al., 2017; Kotwicki et al., 2014; Kłostowska et al., 2018, 2019; Szymczycha et al., 2012, 2020). At four shoreline sites sampled in this study (Figure 1), higher Ra activities were found in combination with lighter $\delta^{2}H_{H2O}$ and $\delta^{13}C_{DIC}$ signatures. At these locations, the sediment porewater salinity of several sites generally showed a concave shape indicating an upward advective groundwater flow of fresh groundwater (Figure 6).

4.2. Early diagenesis and the impact of submarine groundwater discharge on the surface sediments of the Gulf of Gdańsk and Puck Bay

4.2.1. Offshore sites

Site M1 in the Gulf of Gdańsk displayed a decrease in both porewater salinity and the water isotope signatures at depth (Figure 5A), which suggests an upward flow of fresh groundwater. This site is located in an area dominated by clayish silt (Figure 1) with sediments that are characterized by high TOC contents and low C:N ratios (Figure 3A,E) mainly due to the influence of the Vistula River (Szymczak- Żyła and Lubecki 2022). The Hg values in the sediments were constant with depth, possibly due to the high sediment mixing caused by gas flow, as observed at a nearby site by Brodecka-Goluch et al. (2022) and Idczak et al. (2020), and the groundwater discharge.

Also, at this site, intensive organic matter mineralization was observed. Sediment porewater DIC and NH_4 reached concentrations four times higher than the porewaters at the outer Puck Bay sites. Concentrations of SO_4 were already lower in the top sediments due to intense organic matter mineralization combined with the impact of groundwater low in SO_4. Following or overlapping the zone of sulfate reduction, methanogenesis became a pathway for organic matter mineralization already in the surface sediments, confirmed by the heavier values of $\delta^{13}C_{DIC}$ (+14‰). This is commonly observed in coastal settings with high rates of organic matter deposition (Thang et al., 2013). As a result of the low availability of SO_4 and the absence of Fe at the sediment-water interface for possible CH_4 oxidation, CH_4 may easily migrate and impact the bottom waters, as observed by Idczak et al. (2020) at a nearby pockmark. Concentrations of Ba are enriched in the porewaters as has been described by Aloisi et al. (2004) for cold seep sites.

Most of the outer Puck Bay sites, except Site 371330, revealed porewater gradients with constant salinity and uniform concentrations of conservative elements with depth. The surface sediments at these sites are composed of silty clay, clayey silt, and sandy silt (Figure 1). Sediment composition was different between the sites, but the TOC/TS

contents remained below the predicted Holocene saturation line (Figure 5F), indicating sulfate mineralization processes (Berner, 1982; Jørgensen and Kasten, 2006). Most sites showed Hg profiles with enhanced contents at 10 and 20 cmbsf, and thus a relatively continuous sedimentation with little disturbance. In contrast, Site M2 showed constant Hg values with depth, indicating some disturbance probably related to gas outflow. Site M2 is located over an extensive regular shallow gas accumulation (Brodecka-Goluch et al., 2022 and references therein).

The porewater profiles from the outer Puck Bay are shaped by organic matter mineralization and a continuous increase in metabolite concentrations by using, in particular, SO_4 (Figure 5H,I). The $\delta^{13}C_{DIC}$ composition was typical of marine sediments where high rates of mineralization of organic matter are found (Meister et al., 2019). Lighter isotopic signatures in the uppermost sediments at most sites may be indicative of CH_4 oxidation. In addition, no disturbance from bubbles was observed in the acoustic images of the top sediment layer. Porewater displayed high concentrations of the main metabolites originating from organic matter mineralization. Site M2 was impacted by methanogenesis already in the top sediments, as indicated by SO_4 rapidly decreasing to 0, and corresponding $\delta^{13}C_{DIC}$ values that became heavier. Similar to Site M1, this site could also act as a source of CH_4 to the bottom waters.

The low Fe concentrations are probably due to the precipitation of Fe sulfides in the anoxic zone (Balzer, 1982; de Beer et al., 2005). However, in some sites dissolved Fe and Mn were mobilized in the top sediment due to the development of a suboxic zone.

Porewater salinity at Site 371330 displayed a slight decrease in porewater salinity together with the other conservative elements (Figure 5A), suggesting an impact of fresh groundwater in the deeper sediments. This site is located in an area composed mainly of silty clay (Figure 1). The content of TS was lower compared to the other sites in the bay, especially in the top sediments, due to some reoxidation of sedimentary sulfur species such as Fe monosulfides. No substantial bacterial sulfate reduction is observed and therefore H_2S did not accumulate. The lack of H_2S in the porewater may allow higher concentrations of dissolved Fe as no precipitation of Fe phases occurred. Dissolved Fe and Mn were mobilized in the top sediments (Figure 5K,L).

Although Site 371330 showed some freshening with depth, the chemical gradients were similar to the other sites in the outer Puck Bay originating from a strong diagenetic processes.

4.2.2. Shoreline sites

The sediments along the shoreline sites are mainly comprised of medium sandy sediments (Figure 1) and are characterized by low TOC and TS contents (Figure 4G,H) due to their continuous physical reworking, causing clay losses (Morse and Berner, 1995) and intense mineralization of standing stock of organic matter (de Beer et al., 2005). In agreement with these sedimentological features, the porewater gradients (Figure 6) suggest that diffusion is strongly superimposed by porewater advection. Driving forces for this process taking place in the top sediments are bottom currents (Cook et al., 2007; de Beer et al., 2005), and, at SGD-impacted sites, also the upward fluid movements (Billerbeck et al., 2006). These physical processes may be seasonally superimposed to a certain degree by in situ biogeochemical transformations of variable spatial and temporal intensity (Cook et al., 2007).

Porewater salinity displayed a large variability between the study sites. While only some sites showed no or only a slight vertical decrease in salinity (Figure 6, Supplementary Figure 3), most of the sites showed a downward decrease in salinity and reaching freshwater conditions with depth. These sites were chosen to represent the impact of SGD.

The sites with slightly decreasing salinity showed porewater isotopic compositions (δ^2H and $\delta^{18}O$) close to the Baltic Sea signature and were, therefore, not significantly impacted by fresh groundwater. A decrease in pH between 5 and 30 cmbsf accompanied by a slight increase in DIC, indicates active organic matter mineralization probably by sulfate reduction. In addition, some sites were impacted by methanogenesis as the $\delta^{13}C_{DIC}$ reached positive values. Dissolved P, NH_4, and Mn concentrations increased with depth, most likely due to organic matter mineralization. However, the concentration of the metabolites was very low at these sites as the upward advective flow limited the accumulation of these elements in the surface sediments.

Sites with a steeply downward decrease of salinity and porewater isotopic composition indicated clear mixing between the Baltic Sea and the groundwater (Figure 6A–C), indicating the impact of fresh groundwater.

The concentrations of SO_4 dropped down in the top 10 cmbsf due to the influence of fresh groundwater depleted in SO_4. The application of a binary mixing shows a slight SO_4 deficit found in most SGD-impacted porewaters (Supplementary Figure 5), which indicates minor net bacterial sulfate reduction rates (e.g. Donis et al., 2017). Previous investigations further demonstrated the importance of aerobic processes in surface sediments (Cook et al., 2007; Donis et al., 2017).

The concentrations of DIC and the $\delta^{13}C_{DIC}$ signatures indicated different biogeochemical processes (Figure 6F,G). Mixing between fresh groundwater characterized by higher DIC concentrations and lighter and variable $\delta^{13}C_{DIC,}$ and brackish water characterized by lower DIC concentrations and heavier $\delta^{13}C_{DIC}$ composition (Table 1). The mixing is further superimposed by the mineralization of organic matter resulting in lighter $\delta^{13}C_{DIC}$ values (Supplementary Figure 6). In addition, methanogenesis was observed at depth for the Hel Site (Donis et al., 2017; Kotwicki et al., 2014), and possible re-oxidation effects led to shifts towards isotopically lighter stable isotope signatures. In the top sediments, signatures were lighter than those found in the non-SGD-impacted sites, likely indicating possible oxidation of CH_4.

The stable H and C isotope composition of dissolved CH_4 in porewater at the SGD-impacted profiles showed a biogenic origin. They fall within the intermediate region predicted for methanogenesis following the methyl-type fermentation and carbonate reduction pathways (Table 1; Supplementary Figure 4) (e.g., Egger et al., 2017; Whiticar, 1999). Following the classification of Whiticar (1999), the isotope signatures of porewater CH_4 are dominated by the impact of hydrogenotrophic carbonate reduction. A sample close to the sediment-water interface was heavier in both $\delta^{13}C_{CH4}$ and δ^2H_{CH4} than other samples.

This difference is most likely due to the aerobic oxidation of methane in the surface sediment, which has been shown to yield a similar relative isotopic enrichment (Drake et al., 2015).

Concentrations of dissolved nutrients (P, NH_4, and Si) were higher in the SGD-impacted sites compared to the non-impacted sites (Figure 6 J,M,N, Supplementary Figure 6), demonstrating that the fresh SGD component acts as a nutrient source, which is further enhanced by organic matter mineralization. It should also be noted that most elements are expected to flow toward the bottom waters due to the strong upward flow of groundwater, which suppresses the reaction of the elements within the sediments. The higher concentrations of nutrients at SGD sites agree with previous observations (Donis et al., 2017; Szymczycha et al., 2012).

Fe and Mn exceed the concentrations expected based on binary mixing between the bottom and groundwater (Supplementary Figure 5) due to reductive release within the mixing zone of the surface sediments (Balzer, 1982; de Beer et al., 2005). Higher dissolved Fe concentrations were found at two sites impacted by SGD in the inner Puck Bay (Chałupy and Swarzewo, Figure 1), indicating different processes or sedimentary Fe sources for the different sites.

The profiles captured during different seasons of the years 2009 and 2010 did not show a clear seasonal variation between them (Supplementary Figure 3) except for $\delta^{13}C_{DIC}$, which showed some variability associated with different mineralization rates.

4.2.3. Element fluxes

Dissolved constituents in porewater from the 15 selected sites with and without impact by SGD were modeled to estimate the water and element fluxes across the sediment-water interface to learn about the relative importance of diagenesis versus SGD-induced advection (Figure 8, Supplementary Table 3).

Concentrations of Na of the porewaters were used to estimate the groundwater discharge across the sediment-water interface. Using the model approach (section 2.2.3), it was found that the fluxes at the offshore sites (M1, 371330, 371370, M2) are mainly driven by molecular diffusion. The calculated flux of fresh groundwater at Site M1 was 0.005 cm d^{-1} and 0.003 cm d^{-1} for Site 371330. The groundwater flow of the sites where SGD had not been noticed was smaller, about 0.001 cm d^{-1}.

At the sandy shoreline sites, where advective processes shaped the profiles, high groundwater flow was estimated compared to the offshore sites (Figure 8). The modeled groundwater flow at the SGD-impacted sites varied between 0.01 and 0.03 cm d^{-1}. Advection at the non-SGD-impacted sites was found to be much lower and varied in a range of 0 and 0.002 cm d^{-1}.

The associated elemental fluxes were found to vary between the sites as well as they are presented in Supplementary Table 3. The offshore sites were characterized by higher fluxes of DIC, TA, NH_4, and P (Figure 8) out of the sediment, particularly at Site M1, resulting from pronounced organic matter mineralization. These results further highlight the importance of microbial-catalyzed biogeochemical processes for the development of the chemical gradients in the surface sediments.

The elemental fluxes at the sandy shoreline sites were comparatively low despite high advection rates. The calculated fluxes are based on net fluxes, and the advective fluxes might inhibit the accumulation of elements and result in lower element fluxes. However, enhanced fluxes of elements were observed in the profiles impacted by SGD (theoretically, the sites with higher advective flux), suggesting that the groundwater can be a source of these elements and therefore contribute to the addition of elements to surface waters. Moreover, the physical pressure of the upward groundwater flow may facilitate the benthic fluxes at the sediment-water interface.

Despite the lower fluxes obtained, the sandy permeable sediments must be considered when addressing the global cycles of matter as they also represent a source of new or recycled elements to the surface waters (Santos et al., 2012).

4.3. The composition of the submarine groundwater discharge freshwater component: Shoreline sites

The porewater isotopic signatures at the shoreline sites impacted by SGD (Figure 1) were lying on a mixing line between the surface waters of Puck Bay and the groundwaters (Figure 7). The lighter signatures were found at the bottom profile and plotted close to the groundwater signatures (Figure 7).

The SGD-impacted porewater profiles indicate spatial and temporal variability (Supplementary Figure 3). The groundwater-seawater mixing zone moves according to external factors such as wind direction, precipitation, and sea level (Kłostowska et al., 2019; Massel et al., 2004). However, from the salinity gradients, it is possible to roughly estimate that the freshwater composition could be found between 20 and 100 cmbsf at the sandy shoreline sites.

The fresh component of SGD was characterized by extrapolating the profiles to freshwater conditions (the calculation was based on the Mg concentrations in groundwater of 0.4 mM, Table 1). Porewater profiles from Hel, Chałupy, Swarzewo, and Osłonino (Figure 1) were evaluated and compared with values from the groundwater and river water around Puck Bay.

The hydrogeochemical composition of the fresh component of SGD at Hel and Chałupy was Ca-Mg-HCO_3 type, similar to the groundwater and the rivers in this region, and the site in Swarzewo showed some impact by saline water. The fresh component of the SGD on Hel showed a mixed-type composition (Figure 7B).

The Hel site further showed the lightest water isotopic signatures reaching −10.9 and −78.4‰ for $\delta^{18}O_{H2O}$ and $\delta^{2}H_{H2O}$, respectively, which is probably influenced by groundwater from deep aquifers related to the Cretaceous deposits (Piekarek—Jankowska, 1996). The ^{3}H activities found in the porewaters of Hel (Supplementary Table 2) indicate the presence of low/free ^{3}H groundwater. In addition to Hel, a land-based site (Osłonino) appears to be influenced by groundwater from Cretaceous aquifers as implied by the lighter water isotope values (Figure 7).

Although the $\delta^{13}C_{DIC}$ signatures vary over a wide range (Figure 6G, Supplementary Figure 3, L, Supplementary Fig-

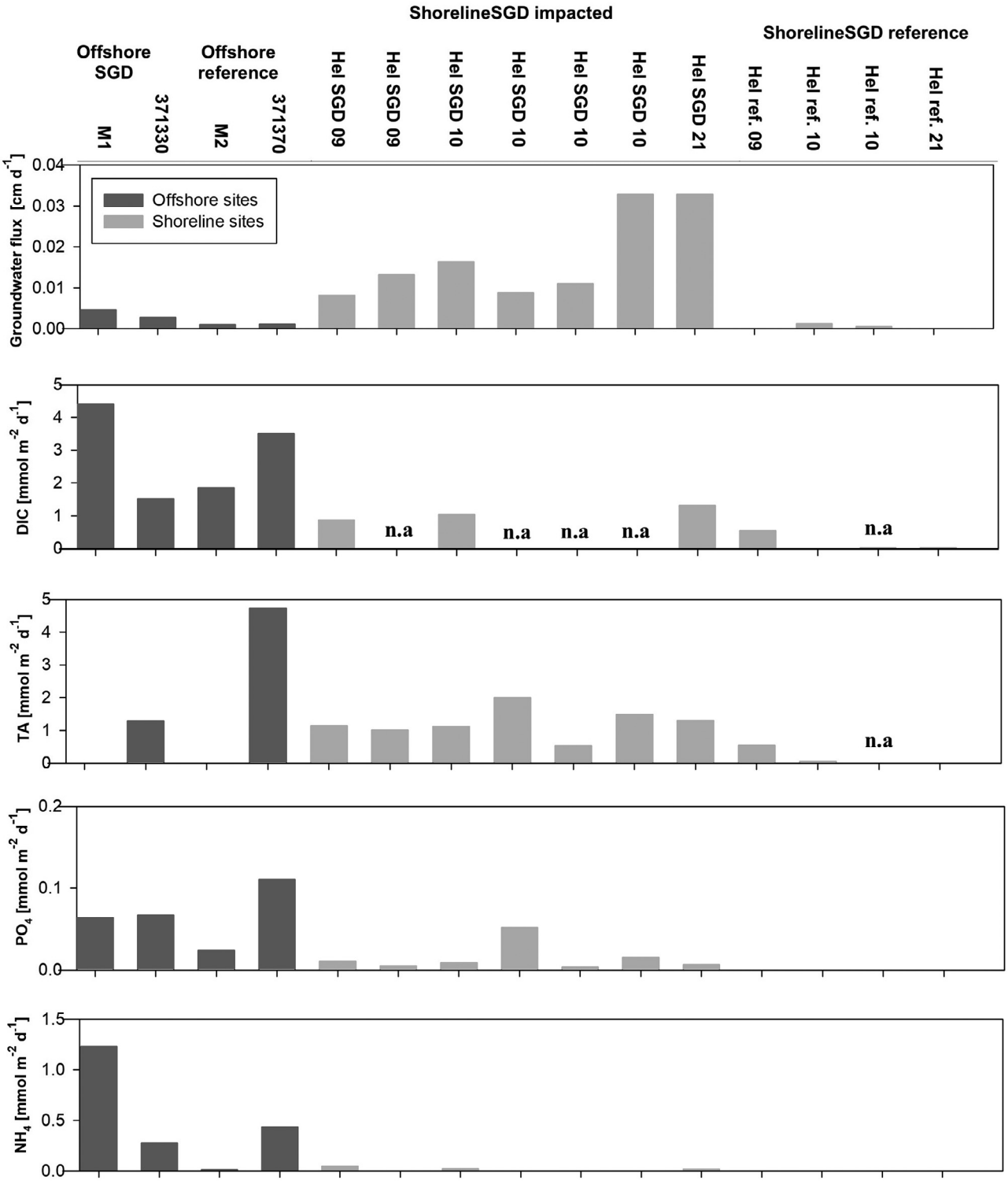

Figure 8 Total fluxes (diffuse + mixing + advective) of water and chemical elements for the offshore muddy SGD and reference sites and selected shoreline sandy SGD and reference sites. The fluxes are presented in Supplementary Table 3.

ure 6, D), the freshwater composition could be calculated to be −19, −16, and −16‰ for Chałupy, Swarzewo and Osłonino, respectively. These values were similar to the signatures found in the deep groundwaters (Table 1), and are probably the result of the mixing of soil CO_2 and C3 Plants, which contribute to the lighter isotopes, and Ca dissolution with the heavier isotopes (e.g. Deines et al., 1974).

4.4. Local and regional estimates of submarine groundwater discharge contribution for the Puck Bay

4.4.1. Local scale of fresh SGD

The modeled groundwater discharge, estimated from the Na gradient, of Site 371330 in the central part of the outer Puck Bay was 0.03 L m^{-2} d^{-1}. Higher groundwater flow estimates were obtained for the shoreline site in Hel, varying between 0.1 and 0.3 L m^{-2} d^{-1}. These estimates refer to the fresh upward groundwater flow.

The SGD fluxes obtained by the seepage meter also include the recirculated component. The fluxes at the Hel shoreline site were between 30 and 45 L m^{-2} d^{-1}. The fluxes obtained for the sites located in the inner part of the Puck Bay, Chałupy, and Swarzewo, were 1.6 and 3.0 L m^{-2} d^{-1}, respectively.

In this study, the seepage fluxes measured with seepage meters are characteristic of the active SGD sites at the shoreline. Estimates from the present study agree with those previously estimated by applying seepage meters ranging from 3 to 187 L m^{-2} d^{-1} (e.g., Donis et al., 2017; Kotwicki et al., 2014; Szymczycha et al., 2012). The fluxes are very heterogeneous because the outflow from the seepage meters is controlled by the geological properties of the selected seafloor (Burnett et al., 2006).

4.4.2. Regional scale SGD

Submarine groundwater discharge is generally a potential source of Ra (Beck et al., 2007b; Charette et al., 2001; Rodellas et al., 2012). In the present study, a Ra isotope mass balance was applied to estimate the total SGD in Puck Bay, following Rodellas et al. (2017). Separate balances for the outer and the inner part of Puck Bay were calculated.

As sources, SGD, rivers, and diffusion from sediments are considered. The sinks are radioactive decay and net export from the study area. Assuming a steady state, the mass balance can be expressed as:

$$Q_{SGD} * Ra_{SGD} + R + F_D - D - O = 0 \quad (4)$$

Where Q_{SGD} is the volumetric SGD (m^3 d^{-1}), Ra_{SGD} is the $^{224}Ra_{ex}$ activity of porewater samples in the study area (Bq m^{-3}). The porewater activities were used as an endmember, since they represent the final solution delivered to the bay. R is the input from rivers (Bq d^{-1}), F_D is the contribution from diffuse fluxes from the sediment (Bq d^{-1}), D is the radioactive decay (Bq d^{-1}) and O is the outflow from the inner and outer Puck Bay (Bq d^{-1}).

The river input is estimated as the product of the discharge and the corresponding $^{224}Ra_{ex}$ activities. The Reda River contributes about 76% of the volume of all rivers discharging into the inner bay (Szymczak and Piekarek-Jankowska, 2007). Therefore, it is considered that the discharge of Zagórska Struga, Gizdepka, and Płutnica together represents 24% of the Reda River discharge.

The diffusive flux determined from the Ra diffusion experiment was multiplied by the area of the bay to obtain F_D.

The radioactive decay is the product of the measured $^{224}Ra_{ex}$ activity of the bay, the volume of the considered part of the bay, and the decay constant.

The outflow was calculated as:

$$O: \frac{(224Ra_{ex}(inner\ or\ outer\ bay) - 224Ra_{ex}(outer\ bay\ or\ Baltic\ Sea)) * V(inner\ or\ outer\ bay)}{WA} \quad (5)$$

Where the WA is the apparent water age, which was estimated by using the short-lived Ra isotopes as described by Moore (2000b):

$$WA: \frac{ln(\frac{224Ra}{223Ra})inner\ or\ outer\ PB - ln(\frac{224Ra}{223Ra})RaSGD}{\lambda 223 - \lambda 224} \quad (6)$$

The Ra-derived estimate of the water age is 4 ± 2 and 15 ± 8 days for the outer and inner parts of Puck Bay, respectively. It should be noted that the water age represents the time elapsed since the water sample became enriched in Ra and was isolated from the source (Moore, 2000b). This application is more appropriate for ages in the range of the half-life of the isotope used.

Considering all the inputs and outputs of the Ra mass balance in the outer Puck Bay, the Q_{SGD} was estimated to be 77 ± 35 10^6 m^3 d^{-1} (301 L m^{-2} d^{-1}) (Table 2). In order to obtain a discharge in the range of the values already estimated for Puck Bay, we estimated that SGD is taking place in the whole bay (255 km^2). This assumption could be realistic to some extent as acoustic imagery showed anomalies in the surface sediments (Figure 3) and salinity in the water column decreased with depth at some sites (Matciak et al., 2015). However, the SGD fluxes estimated here are the sum of the fresh and saline components of SGD, and a balance using long-lived Ra isotopes is required to differentiate between porewater exchange and SGD (Rodellas et al., 2017).

Considering the $^{224}Ra_{ex}$ sources to the outer bay, the SGD represents 94%, whereas the outflow from the inner Puck Bay represents and the diffusion each account for only 3%. In this balance, the Vistula River is not considered as a source of Ra to Puck Bay, which could have an impact depending on the wind direction. Moreover, the contribution from the sediments could also be higher if the diffusion experiment was done for the different sediments found across the bay.

Regarding the inner Puck Bay, Q_{SGD} was estimated to be 6 ±6 10^6 m^3 d^{-1} (55 L m^{-2} d^{-1}) (Table 2). As assumed in the outer Puck Bay, we assume that SGD occurs in the entire inner bay (104 km^2) as well. Here, SGD dominates again with 91%, rivers 0.5%, and diffusion represents 9%.

It is worth noting that the present balances have high levels of uncertainties. Among the factors, the Ra activities found in the end members were very heterogeneous showing a wide range of activities between them. Salinity has been recognized as the main factor controlling the activities in the endmembers since Ra desorption increases with salinity (e.g. Cho and Kim, 2016). In addition, high variability was observed in the $^{224}Ra_{ex}$ activities of the groundwaters around Puck Bay, which ranged between 0 and 14 Bq m^{-3} (Table 1), which suggests that the groundwater discharging into Puck Bay may be formed and flow through a different lithology.

The SGD in the inner part of Puck Bay was found to be about 24 times higher than the discharge of the Reda River on the day of sampling (3 m^3 s^{-1}, IMGW, 2022).

Table 2 Summary of the terms and values used in the Ra mass balance.

Term	Definition	Outer Puck Bay	Inner Puck Bay	Source
A	Area of the bay [m^2]	255200000	104000000	Kramarska et al. (1995)
V	Volume of the bay [m^3]	5231600000	322400000	Szymczak and Szmytkiewicz (2014)
h	average depht of the bay [m]	20.5	3	Matciak et al. (2011)
Q_{rivers}	Total discharge of Gizdepka, Plutnica and Zagorska Struga rivers [m^3 d^{-1}]		73667.37	24% of Reda discharge Szymczak and Piekarek-Jankowska (2007), IMGW (2022)
Q_{Reda}	Discharge of Reda River [m^3 d^{-1}]		233280	IMGW (2022)
λ224	$^{224}Ra_{ex}$ decay constant [d^{-1}]	0.19	0.19	
λ223	$^{223}Ra_{ex}$ decay constant [d^{-1}]	0.06	0.06	
WA	Water age [d]	4	15	Eq. (6)
Ra_{Reda}	$^{224}Ra_{ex}$ concentration in Reda River [Bq m^{-3}]		2.2	this study
Ra_{rivers}	$^{224}Ra_{ex}$ activties in the Gizdepka River [Bq m^{-3}]		0.5	this study
Ra_{rivers}	$^{224}Ra_{ex}$ concentration in the Płutnica River [Bq m^{-3}]		0.9	this study
Ra_{rivers}	$^{224}Ra_{ex}$ concentration in the Zagórska Struga River [Bq m^{-3}]		1	this study
$Ra_{Baltic\ Sea}$	$^{224}Ra_{ex}$ concentration in the Baltic Sea site [Bq m^{-3}]	0.3		this study
$Ra_{outer\ PB}$	Average $^{224}Ra_{ex}$ concentration in the Outer Puck Bay [Bq m^{-3}]	0.5	0.5	this study
$Ra_{inner\ PB}$	Average of $^{224}Ra_{ex}$ in the inner Puck Bay [Bq m^{-3}]	1.6	1.6	this study
F_{dif}	Ra flux out from bottom sediments [Bq m^{-2} d^{-1}]	0.1	0	this study
Ra_{SGD}	$^{224}Ra_{ex}$ of porewater Sopot (SGD) [Bq m^{-3}]	13.6		this study
Ra_{SGD}	$^{224}Ra_{ex}$ of porewater Hel (SGD) [Bq m^{-3}]	7		this study
Ra_{SGD}	$^{224}Ra_{ex}$ of porewater Chalupy (SGD) [Bq m^{-3}]		31	this study
Ra_{SGD}	$^{224}Ra_{ex}$ of porewater Swarzeno (SGD) [Bq m^{-3}]		9	this study
Ra_{SGD}	$^{224}Ra_{ex}$ of porewater Oslonino (SGD) [Bq m^{-3}]		79	this study

Term	Calculations	Outer Puck Bay	Inner Puck Bay	Source
O	Ra output fluxes [Bq d^{-1}]	261580000	23642667	Eq. (5)
D	Radioactive decay [Bq d^{-1}]	497002000	98009600	$^{224}Ra_{ex}PB*V*λ224$, Rodellas et al. (2017)
R	contribution from the inner Puck Bay [Bq d^{-1}]	23642667		Eq. (5)
R	contribution from rivers [Bq d^{-1}]		572150	(Q_{rivers} * average of Ra_{rivers}) + (Q_{Reda}* Ra_{Reda})
F_D	contribution from diffuse fluxes out of bottom sediments [Bq d^{-1}]	25520000	10400000	F_{dif} * A
Q_{SGD}*Ra_{SGD}	contribution from SGD [Bq d^{-1}]	640362213	106424437	$(D + O) - (R + F_D)$
Q_{SGD}	Flux of SGD [10^6 m^3 d^{-1}]	77	6	Balance/Ra_{SGD}
Q_{SGD}	Flux of SGD per area [L m^{-2} d^{-1}]	301	55	Q_{SGD}/A

Table 3 Information of SGD fluxes estimated in different studies for Puck Bay, and, for some sites along the Baltic Sea.

Location	Year sampling	Approach	Discharge [L m^{-2} d^{-1}]	Reference
Puck Bay	1994	only Fresh SGD	0.4	Piekarek—Jankowska (1994, 1996)
Hel — outer Puck Bay	2009—2010	Seepage meter	3—22	Szymczycha et al. (2012)
Hel — outer Puck Bay	2009/2010	Benthic seepage meters	10 —150	Kotwicki et al. (2014)
Hel — outer Puck Bay	2009	Benthic chamber	86 ±16	Donis et al. (2017)
outer Puck Bay (Hel, Jurata, Swarzewo, and Puck)	2017/2018	Chloride tracer	156—242	Kłostowska et al. (2019)
inner Puck Bay (Chałupy and Osłonino)	2017/2018	Chloride tracer	156—242	Kłostowska et al. (2019)
Hel — outer Puck Bay	2021	Seepage meter	30—45	This study
Chalupy — inner Puck Bay	2021	Seepage meter	2	This study
Swarzewo — inner Puck Bay	2021	Seepage meter	3	This study
Site 371330 — outer Puck Bay	2009	Na profile - only fresh SGD	0.003	This study
Hel — outer Puck Bay	2009—2021	Na profile	0.01—0.03	This study
outer Puck Bay	2019	Ra isotopes	301	This study
inner Puck Bay	2021	Ra isotopes	55	This study
Gulf of Finland		geological and hydrogeological methods	0.1	Viventsova and Voronov (2003)
Eckernforde Bay, Germany	1998/2001	Chloride tracer	<9	Schlüter et al. (2004)
Forsmark, Gulf of Bothnia	2013	Ra isotopes	0.3—59	Krall et al. (2017)

The estimates from the Ra mass balance are overall in agreement with those measured by seepage meters or porewater profiles (this study, Donis et al., 2017; Kłostowska et al., 2019; Kotwicki et al., 2014; Szymczycha et al., 2012, Supplementary Table 2). This regional approach based on Ra isotopes further provides for the first time an integrated estimate of the SGD over the whole Puck Bay area.

The different methods used in this study proved that SGD is taking place with high spatial heterogeneity and a wider range in the volumetric and elemental fluxes. The variability is due to the fact that SGD is a local phenomenon, and the calculations are subject to assumptions and uncertainties depending on the number of active SGD sites, which is still unknown. In addition, our values exceed those reported for other regions of the Baltic Sea due to the favorable geological, sedimentological and/or hydrological conditions for SGD in the Puck Bay (Table 3).

5. Conclusions

Puck Bay can be considered a hotspot for submarine groundwater discharge compared to other coastal areas of the Baltic Sea. The current multi-method approach applied to the water column, porewater, and sediment samples identified SGD mainly along the sandy shoreline, but also in the deeper central part of Puck Bay.

Local and regional SGD fluxes derived from seepage meters measurements and a Ra isotope mass balance yielded values between 3 and 300 L m^{-2} d^{-1}. Fluxes of SGD at sandy sites clearly exceed the values determined at muddy sites. Elemental fluxes across the sediment-water interface of organic-rich muds (impacted and non-impacted sites) were found to be driven by early diagenesis and were higher at the muddy sites. The SGD-impacted sandy sites showed intense mixing between upward-moving freshwater and seawater, and early diagenetic processes were less pronounced in shaping the porewater gradients. SGD leads to the release of DIC and TA into the bottom waters. The carbon isotopic composition of DIC shows temporal changes, likely driven by changes in the availability and re-oxidation of biogenic CH_4. This indicates that CH_4 is probably not derived from the original aquifer, but rather from a zone between the deeper aquifer and the overlying sands. Our approach enabled the detection of different freshwater endmembers originating from different aquifers. It also indicates that the SGD-derived chemical fluxes strongly depend on the composition and processes occurring in the surface sediments.

Therefore, future studies need to take into account the non-conservative behavior of constituents in subterranean estuaries in order to better resolve the potentially important quantitative role of SGD in coastal areas. Moreover, climate and land-use changes should be considered, for instance sea level rise, land uplift, wind pattern and the amount of precipitation which can modify the hydraulic gradient between the land and the ocean, and thus the direction, velocity and composition of the SGD flows.

Declaration of competing interest

The authors declare that they have no known competing financial interests or personal relationships that could have appeared to influence the work reported in this paper.

Acknowledgments

The authors wish to thank the staff at the Hel Marine Station (Institute of Oceanography, University of Gdańsk) for their continuous support during the field campaigns and the stimulating working atmosphere. We also thank the crew and captain of r/vs *Professor Albrecht Penck* and *Oceania* for technical support. Karol Kuliński, Jacek Bełdowski, Maciej Chełchowski, Marta Borecka, Monika Lengier, Piotr Balazy, and Seyed Reza Saghravani are thanked for the support during the fieldwork. Anne Köhler, Ines Scherff, and Dagmar Benesch from IOW and Marta Borecka from IOPAN are thanked for their expert support in the laboratory. Jacek Urbański for the help with the study area map. Jan Scholten and Patricia Roeser are thanked for the insightfull discussions, that helped to improve this manuscript. The water utility companies: "Saur Neptun Gdańsk", "Pucka Gospodarka Komunalna", MPWiK "EKOWIK", "PEWIK GDYNIA", "EKO-HEL BIS", especially Radosław Walczak, Konrad Krampichowski, Julia Nowak, Jarosław Myślisz, Michał Twardowski, Zbigniew Rydz, and all staff members are thanked for their support during groundwater sampling.

Funding

Financial support for this work was provided by a DAAD stipend to CMEvA (Doctoral program in Germany 2018/2019, project no. 57381412), to MEB by the BONUS+ project AMBER (BMBF project No.03F0485A), the European Union's Horizon 2020 research and innovation programme under grant agreement no. 730984 (Assemble Plus project), and the Leibniz Institute for Baltic Sea Research. It was furthermore supported to BS by the Institute of Oceanology Polish Academy of Sciences (IOPAN) and project nr.2019/34/E/ST10/00217 funded by the Polish National Science Centre. This work was conducted within the framework of the Research Training Group "Baltic TRANSCOAST" funded by the DFG (Deutsche Forschungsgemeinschaft) under the grant GRK 2000 (www.baltic-transcoast.uni-rostock.de) . This is Baltic TRANSCOAST publication no. GRK2000/0068.

Data availability

The raw data supporting the conclusions of this article will be made available by the authors via the PANGEA database. Further information will be made available by the authors upon request.

Supplementary materials

Supplementary material associated with this article can be found, in the online version, at https://doi.org/10.1016/j.oceano.2024.01.001.

References

Aloisi, G., Wallmann, K., Bollwerk, S., Derkachev, A., Bohrman, G., Suess, E., 2004. The effect of dissolved barium on biogeochemical processes at cold seeps. Geochim. Cosmochim. Ac. 68, 1735—1748.

Atlas of Polish marine area bottom habitats, 2009. Atlas of Polish marine area bottom habitats. Environmental valorization of marine habitats. Institute of Oceanology PAN, Available at:. https://www.iopan.gda.pl/hm/atlas/Atlas_all.pdf.

Balzer, W., 1982. On the distribution of iron and manganese at the sediment/water interface: thermodynamic versus kinetic control. Geochim. Cosmochim. Ac. 46, 1153—1161. https://doi.org/10.1016/0016-7037(82)90001-1

Beck, A.J., Rapaglia, J.P., Cochran, K., Bokuniewicz, H.J., 2007a. Radium mass-balance in Jamaica Bay, NY: Evidence for a substantial flux of submarine groundwater. Mar. Chem. 106, 419—441. https://doi.org/10.1016/j.marchem.2007.03.008

Beck, A.J., Tsukamoto, Y., Tovar-Sanchez, T., Huerta-Diaz, M., Bokuniewicz, H.J., Sanudo-Wilhelmy, S.A., 2007b. Importance of geochemical transformations in determining submarine groundwater discharge-derived trace metal and nutrient fluxes. Appl. Geochem. 22, 477—490. https://doi.org/10.1016/j.apgeochem.2006.10.005

Berner, R.A., 1982. Burial of organic carbon and Pyrite sulfur in the modern ocean: its geochemical and environmental significance. Am. J. Sci. 282 (4), 451—473. https://doi.org/10.2475/ajs.282.4.451

Berner, R.A., Raiswell, R., 1983. Burial of organic carbon and pyrite sulfur in sediments over Phanerozoic Time: a new theory. Geochim. Cosmochim. Ac. 47 (5), 855—862. https://doi.org/10.1016/0016-7037(83)90151-5

Billerbeck, M., Werner, U., Bosselmann, K., Walpersdorf, E., Huettel, M., 2006. Nutrient release from an exposed intertidal sand flat. Mar. Ecol. Prog. Ser. 316, 35—51.

Boudreau, B.P., 1997. Diagenetic models and their implementation: Modelling transport and reactions in aquatic sediments. Springer-Verlag, Berlin, Heidelberg, New York, 414 pp.

Blöschl, G., Bierkens, M.F.P., Chambel, A., Cudennec, C., Destouni, G., Fiori, A., et al., 2019. Twenty-three Unsolved Problems in Hydrology (UPH) — a Community Perspective. Hydrolog. Sci. J. 64, 1141—1158. https://doi.org/10.1080/02626667.2019.1620507

Böttcher, M.E., Lipka, M., Winde, V., Dellwig, O., Böttcher, E.O., Böttcher, T.M.C., Schmiedinger, I., 2014. Multi-isotope composition of freshwater sources for the southern North and Baltic Sea. In: Proc. 23rd SWIM conference, Husum, 46—49.

Böttcher, M.E., Schmiedinger, I., 2021. The Impact of Temperature on the Water Isotope ($^{2}H/^{1}H$, $^{17}O/^{16}O$, $^{18}O/^{16}O$) Fractionation upon Transport through a Low-Density Polyethylene Membrane. Isot. Environ. Healt. S. 57, 183—192. https://doi.org/10.1080/10256016.2020.1845668

Böttcher, M.E., Mallast, U., Massmann, G., Moosdorf, N., Mueller-Petke, M., Waska, H., 2024. Coastal-Groundwater Interfaces (Submarine Groundwater Discharge). In: Krause, S., Hannah, D.M., Grimm, N. (Eds.), Ecohydrological Interfaces. Wiley & Sons, New York, 123—148.

Brand, W.A., Coplen, T.B., 2012. Stable isotope deltas: tiny, yet robust signatures in nature. Isotopes Environ. Health Stud. 48, 393—409. https://doi.org/10.1080/10256016.2012.666977

Brodecka-Goluch, A., Lukawska-Matuszewska, L., Kotarba, M.J., Borkowski, A., Idczak, J., Bolalek, J., 2022. Biogeochemistry of three different shallow gas systems in continental shelf sediments of the South-Eastern Baltic Sea (Gulf of Gdańsk): Carbon cycling, origin of methane and microbial community composition. Chem. Geol. 597, 120799. https://doi.org/10.1016/j.chemgeo.2022.120799

Burnett, W.C., Bokuniewicz, H., Huettel, M., Moore, W.S., Tamiguchi, M., 2003. Groundwater and porewater inputs to the coastal zone. Biogeochemistry 66, 3—33.

Burnett, W.C., Aggarwal, P.K., Aureli, A., Bokuniewicz, H., Cable, J.E., Charette, M.A., Kontar, E., Krupa, S., Kulkarni, K.M., Loveless, A., Moore, W.S., Oberdorfer, J.A., Oliveira, J., Ozyurt, N., Povinec, P., Privitera, A.M.G., Rajar, R., Ramessur, R.T., Turner, J.V., 2006. Quantifying Submarine Groundwater Discharge in the Coastal Zone via Multiple Methods. Sci. Total. Environ. 367, 498—543. https://doi.org/10.1016/j.scitotenv.2006.05.009

Cerdà-Domènech, M., Rodellas, V., Folch, A., Garcia-Orellana, J., 2017. Constraining the temporal variations of Ra isotopes and Rn in the groundwater end-member: Implications for derived SGD estimates. Sci. Total. Environ. 595, 849—857. https://doi.org/10.1016/j.scitotenv.2017.03.005

Charette, M.A, Buesseler, K., Andrews, J., 2001. Utility of radium isotopes for evaluating the input and transport of groundwater-derived nitrogen to a Cape Cod estuary. Limnol. Oceanogr. 46 (2), 465—470. https://doi.org/10.4319/lo.2001.46.2.0465

Charette, M.A., Sholkovitz, E.R., Hansel, C.M., 2005. Trace element cycling in a subterranean estuary Part 1. Geochemistry of the permeable sediments. Geochim. Cosmochim. Ac. 69 (8), 2095—2109. https://doi.org/10.1016/j.gca.2004.10.024

Cho, H-M., Kim, G., 2016. Determining groundwater Ra end-member values for the estimation of the magnitude of submarine groundwater discharge using Ra isotope tracers. Geophys. Res. Let. 43 (8), 3865—3871. https://doi.org/10.1002/2016GL068805

Church, T., 1996. An underground route for the water cycle. Nature 380, 579 pp.

Cline, J.D., 1969. Spectrophotometric Determination of Hydrogen Sulfide in Natural Waters. Limnol. Oceanogr. 14, 454—458.

Cook, P.L.M., Wenzhöfer, F., Glud, R.N., Janssen, F., Huettel, M., 2007. Benthic solute exchange and carbon mineralization in two shallow subtidal sandy sediments: Effect of advective porewater exchange. Limnol. Oceanogr. 52, 1943—1963. https://doi.org/10.4319/lo.2007.52.5.1943

de Beer, D., Wenzhöfer, F., Ferdelman, T.G., Boehme, S.E., Huettel, M., van Beusekom, J.E.E., Böttcher, M.E., Musat, N., Dubilier, N., 2005. Transport and mineralization rates in North Sea sandy intertidal sediments, Sylt-Rømø basin, Wadden Sea. Limnol. Oceanogr. 50 (1), 113—127. https://doi.org/10.4319/lo.2005.50.1.0113

Deines, P., Langmuir, D., Harmon, R.S., 1974. Stable carbon isotope ratios and the existence of a gas phase in the evolution of carbonate ground waters. Geochim. Cosmochim. Ac. 38, 1147—1164. https://doi.org/10.1016/0016-7037(74)90010-6

Dippner, J.W., Bartl, I., Chrysagi, E., Holtermann, P., Kremp, A., Thoms, F., Voss, M., 2019. Lagrangian Residence Time in the Bay of Gdańsk, Baltic Sea. Front. Mar. Sci. 6, 725. https://doi.org/10.3389/fmars.2019.00725

Drake, H., Åström, M., Heim, C., Broman, C., Åström, J., Whitehouse, M., Ivarsson, M., Siljeström, S., Sjövall, 2015. Extreme 13C depletion of carbonates formed during oxidation of biogenic methane in fractured granite. Nat. Commun. 6, 7020. https://doi.org/10.1038/ncomms8020

Donis, D., Janssen, F., Liu, B., Wenzhöfer, F., Dellwig, O., Escher, P., Spitzy, A., Böttcher, M.E., 2017. Biogeochemical impact of submarine groundwater discharge on coastal surface sands of the southern Baltic Sea. Estuar. Coast. Shelf Sci. 189, 131—142. https://doi.org/10.1016/j.ecss.2017.03.003

Egger, M., Hagens, M., Sapart, C.J., Dijkstra, N., van Helmond, N.A.G.M., Mogollón, J., Risgaard-Petersen, N., van der Veen, C., Kasten, S., Riedinger, N., Böttcher, M.E., Röckmann, T., Jørgensen, B.B., Slomp, C.P., 2017. Iron oxide reduction in methane-rich deep Baltic Sea sediments. Geochim. Cosmochim. Ac. 207, 256—276. https://doi.org/10.1016/j.gca.2017.03.019

Ehlert von Ahn, C.M., Böttcher, M.E., Malik, C., Westphal, J., Rach, B., Nantke, C.K., Jenner, A., Saban, R., Winde, V., Schmiedinger, I., 2023. Spatial and temporal variations in the isotope hydrobiogeochemistry of a managed river draining towards the southern Baltic Sea. Geochemistry 83 (3), 125979. https://doi.org/10.1016/j.chemer.2023.125979

EEA. European Environment Agency. Data and Maps. EEA coastline. available at: http://www.eea.europa.eu/data-and-maps/data/eea-coastline-for-analysis-2/gis-data/eea-coastline-polygon/@@rdf (accessed at 22.10.2022).

Falkowska, L., Piekarek-Jankowska, H., 1999. Submarine seepage of fresh groundwater: disturbance in hydrological and chemical structure of the water column in the Gdańsk Basin. ICES J Mar. Sci. 56, 153—160. https://doi.org/10.1016/j.jmarsys.2013.06.009

Froelich, P.N., Klinkhammer, G.P., Bender, M.L., Luedtke, N.A., Heath, G.R., Cullen, D., Dauphin, P., Hammond, D., Hartman, B., Maynard, V., 1979. Early oxidation of organic matter in pelagic sediments of the eastern equatorial Atlantic: Suboxic diagenesis. Geochim. Cosmochim. Ac. 43, 1075e1090. https://doi.org/10.1016/0016-7037(79)90095-4

Garcia-Solsona, E., Garcia-Orellana, J., Masqué, P., Dulaiova, H., 2008. Uncertainties Associated with ^{223}Ra and ^{224}Ra Measurements in Water via a Delayed Coincidence Counter (RaDeCC). Mar. Chem. 109, 198—219. https://doi.org/10.1016/j.marchem.2007.11.006

Gat, J.R., 1996. Oxygen and hydrogen isotopes in the hydrologic cycle. Annu. Rev. Earth Planet. Sci. 24, 225—262. https://doi.org/10.1146/annurev.earth.24.1.225

Goyetche, T., Luquot, L., Carrera, J., Martínez-Pérez, L., Folch, A., 2022. Indentification and quantification of chemical reactions in a coastal aquifer to assess submarine groundwater discharge composition. Sci. Total. Environ. 838 (1), 155978. https://doi.org/10.1016/j.scitotenv.2022.155978

Grasshoff, K., Kremling, K., Ehrhardt, M., 2009. Methods of Seawater Analysis. Wiley & Sons, Weinheim, 600 pp.

Gupta, P., Noone, D., Galewsky, J., Sweeney, C., Vaughn, B.H., 2009. Demonstration of high-precision continuous measurements of water vapor isotopologues in laboratory and remote field deployments using wavelength-scanned cavity ring-down spectroscopy (WS-CRDS) technology. Rapid Commun. Mass Sp. 23, 2534—2542. https://doi.org/10.1002/rcm.4100

HELCOM. River and lake outlines around the Baltic Sea based on 1:1,000,000 scale source maps. available at: https://metadata.helcom.fi/geonetwork/srv/eng/catalog.search#/metadata/f0edff62-d9fa-4fda-9b42-da3947ee248a. (accessed at 22.05.2022).

Hoffmann, J.J.L., von Deimling, J.S., Schröder, J.F., Schmidt, M., Held, P., Crutchley, G.J., Scholten, J., Gorman, A.R., 2020. Complex Eyed pockmarks and submarine groundwater discharge revealed by acoustic data and sediment cores in Eckernförde Bay. SW Baltic Sea. Geochem. Geophy. Geosy. 21, e2019GC008825. https://doi.org/10.1029/2019GC008825

Hovland, M., Talbot, M., Olaussen, S., Aasberg, L., 1987. Methane-related carbonate cements in pockmarks of the North Sea. J. Sediment. Res. 57 (5), 881—892. https://doi.org/10.1306/212f8c92-2b24-11d7-8648000102c1865d

Huettel, M., Ziebis, W., Forster, S., Luther, W., 1998. Advective transport affecting metal and nutrient distributions and interfacial fluxes in permeable sediments. Geochim. Cosmochim. Ac. 62 (4), 613—631. https://doi.org/10.1016/S0016-7037(97)00371-2

IMGW, 2022. The data have been processed at the Institute of Meteorology and water management — National Research Institute Poland.

Idczak, J., Brodeck-Goluch, A., Lukawska-Matuszewska, K.,

Graca, B., Gorska, N., Klusek, Z., Pezacki, P.D., Bolalek, J., 2020. A geophysical, geochemical and microbiological study of a newly discovered pockmark with active gas seepage and submarine groundwater discharge (MET1-BH, central Gulf of Gdańsk, southern Baltic Sea). Sci. Total. Environ. 742, 140306. https://doi.org/10.1016/j.scitotenv.2020.140306

Iversen, N., Jørgensen, B.B., 1985. Anaerobic methane oxidation rates at the sulfate-methane transition in marine sediments from Kattegat and Skagerrak (Denmark). Limnol. Oceanogr. 30 (5), 944—955. https://doi.org/10.4319/lo.1985.30.5.0944

Jørgensen, B.B., Böttcher, M.E., Lüschen, H., Neretin, L.N., Volkov, I.I., 2004. Anaerobic methane oxidation and a deep H_2S sink generate isotopically heavy sulfides in Black Sea sediments. Geochim. Cosmochim. Ac. 68 (9), 2095—2118. https://doi.org/10.1016/j.gca.2003.07.017

Jørgensen, B.B., Kasten, S., 2006. Sulfur cycling and methane oxidation. In: Schulz, H.D., Zabel, M. (Eds.), Marine Geochemistry. Springer-Verlag, Berlin, Heidelberg, 271—309.

Jurasinski, G., Janssen, M., Voss, M., Böttcher, M.E., Brede, M., Burchard, H., Forster, S., Gosch, L., Gräwe, U., Gründling-Pfaff, S., Haider, F., Ibenthal, M., Karow, N., Karsten, U., Kreuzburg, M., Lange, X., Langer, S., Leinweber, P., Rezanezhad, F., Rehder, G., Romoth, K., Schade, H., Schubert, H., Schulz-Vogt, H., Sokolova, I., Strehse, R., Unger, V., Westphal, J., Lennartz, B., 2018. Understanding the Coastal ecocline: Assessing sea-land-interactions at non-tidal, low-lying coasts through interdisciplinary research. Front. Mar. Sci. 5, 1—22. https://doi.org/10.3389/fmars.2018.00342

Kłostowska, Z., Szymczycha, B., Kuliński, K., Lengier, M., Łęczyński, L., 2018. Hydrochemical characterization of various groundwater and seepage water resources located in the Bay of Puck, Southern Baltic Sea. E3S Web of Conferences 54, 00013. https://doi.org/10.1051/e3sconf/20185400013

Kłostowska, Z., Szymczycha, B., Lengier, M., Zarzeczanska, D., Dzierzbicka-Glowacka, L., 2019. Hydrogeochemistry and magnitude of SGD in the Bay of Puck, southern Baltic. Oceanologia 62 (1), 1—11. https://doi.org/10.1016/j.oceano.2019.09.001

Krall, L., Garcia-Orellana, J., Trezzi, G., Rodellas, V., 2017. Submarine Groundwater Discharge at Forsmark, Gulf of Bothnia, provided by Ra Isotopes. Mar. Chem. 162, 162—172.

Kramarska, R., Uscinowicz, S., Zachowicz, J., Kawinska, M., 1995. Origin and Evolution of the Puck Lagoon. J. Coast. Res. 22, 187—191. https://doi.org/10.1016/j.marchem.2017.09.003

Kotwicki, L., Grzelak, K., Czub, M., Dellwig, O., Gentz, T., Szymczycha, B., Böttcher, M.E., 2014. Submarine groundwater discharge to the Baltic coastal zone: Impacts on the meiofaunal community. J. Marine Syst. 129, 118—126. https://doi.org/10.1016/j.jmarsys.2013.06.009

Leipe, T., Moros, M., Kotilainen, A., Vallius, H., Kabel, K., Endler, M., Kowalski, N., 2013. Mercury in Baltic Sea Sediments — Natural Background and Anthropogenic Impact. Geochemistry 73, 249—259. https://doi.org/10.1016/j.chemer.2013.06.005

Löffler, H., Adam, C., Brinschwitz, D., Gieseler, W., Ginzel, G., Grunske, K.-A., Heeger, D., Meinert, N., Nillert, P., Richter, C., Victor, N., 2010. Hydrochemische Typisierung für Grundwasser im Lockergestein Bereich des norddeutschen Flachlandes. Schriftenreihe für Geowissenschaften 18, 369—399.

Majewski, A., 1990. The Gulf of Gdańsk. Wydawnictwo Geologiczne, Warsaw, (in Polish).

Massel, S.R., Przyborska, A., Przyborski, M., 2004. Attenuation of wave-induced groundwater pressure in shallow water. Part 1. Oceanologia 46 (3), 383—404.

Matciak, M., Nowacki, J., Krzyminski, W., 2011. Upwelling intrusion into shallow Puck Lagoon, a part of Puck Bay (the Baltic Sea). Oceanol. Hydrobiol. St. 40, 2. https://doi.org/10.2478/s13545-011-0021-8

Matciak, M., Bieleninik, S., Botur, A., Podgórski, M., Trzcinska, K., Draganska, K., Jasniewicz, D., Kurszewska, A., Wenta, M., 2015. Observations of presumable groundwater seepage occurrence in Puck Bay (the Baltic Sea). Oceanol. Hydrobiol. St. 44 (2), 267—272. https://doi.org/10.1515/ohs-2015-0025

Mayfield, K.K., Eisenhauer, A., Ramos, D.P.S., Higgins, J.A., Horner, T.J., Auro, M., Magna, T., Moosdorf, N., Charette, M.A., Gonneea, M.E., Brady, C.E., Komar, N., Peucker-Ehrenbrink, B., Paytan, A., 2021. Groundwater discharge impacts marine isotope budgets of Li, Mg, Ca, Sr, and Ba. Nat. Commun. 12, 148. https://doi.org/10.1038/s41467-020-20248-3

Meister, P., Liu, B., Khalili, A., Böttcher, M.E., Jørgensen, B.B., 2019. Factors controlling the carbon isotope composition of dissolved inorganic carbon and methane in marine porewater: An evaluation by reaction transport modelling. J. Marine Syst. 200, 103227. https://doi.org/10.1016/j.jmarsys.2019.103227

Moore, W.S., 1996. Large groundwater inputs to coastal waters revealed by ^{226}Ra enrichments. Nature 380, 612—614. https://doi.org/10.1038/380612a0

Moore, W.S., Arnold, R., 1996. Measurement of ^{223}Ra and ^{224}Ra in Coastal Waters Using a Delayed Coincidence Counter. J. Geophys. Res. 101, 1321—1329. https://doi.org/10.1029/95JC03139

Moore, W.S., 1999. The subterranean estuary: a reaction zone of ground water and sea water. Mar. Chem. 65, 111—125. https://doi.org/10.1016/S0304-4203(99)00014-6

Moore, W.S., 2000a. Determining coastal mixing rates using radium isotopes. Cont. Shelf Res. 20, 1993—2007. https://doi.org/10.1016/S0278-4343(00)00054-6

Moore, W.S., 2000b. Ages of continental shelf waters determined from ^{223}Ra and ^{224}Ra. J. Geophys. Res. 105, 22117—22122. https://doi.org/10.1029/1999JC000289

Moore, W.S., 2006. Radium isotopes as tracers of submarine groundwater discharge in Sicily. Cont. Shelf. Res. 26, 852—861. https://doi.org/10.1016/j.csr.2005.12.004

Moore, W.S., 2010. The effect of submarine groundwater discharge on the Ocean. Annu. Rev. Mar. Sci. 2, 59—88. https://doi.org/10.1146/annurev-marine-120308-081019

Moore, W.S., Beck, M., Riedel, T., Rutgers van der Loeff, M., Dellwig, O., Shaw, T.J., Schnetger, B., Brumsack, H.-J., 2011. Radium-based pore water fluxes of silica, alkalinity, manganese, DOC, and uranium: A decade of studies in the German Wadden Sea. Geochim. Cosmochim. Ac. 75, 6535—6555. https://doi.org/10.1016/j.gca.2011.08.037

Moosdorf, N., Böttcher, M.E., Adyasari, D., Erkul, E., Gilfedder, B.S., Greskowiak, J., Jenner, A-K., Kotwicki, L., Massmann, G., Müller-Petke, M., Oehler, T., Post, V., Prien, R., Scholten, J., Siemon, B., Ehlert von Ahn, C.M., Walther, M., Waska, H., Wunderlich, T., Mallast, U., 2021. A State-Of-The-Art Perspective on the Characterization of Subterranean Estuaries at the Regional Scale. Front. Earth Sci. 9, 601293, 1—26. https://doi.org/10.3389/feart.2021.601293

Morse, J.W., Berner, R.A., 1995. What determines sedimentary C/S ratios? Geochim. Cosmochim. Ac. 59 (6), 1073—1077. https://doi.org/10.1016/0016-7037(95)00024-T

Oberdorfer, J.A., Charette, M., Allen, M., Martin, J.B., Cable, J.E., 2008. Hydrogeology and geochemistry of near-shore submarine groundwater discharge at Flamendo Bay, Ubatuba, Brazil. Estuar. Coast. Shelf Sci. 76, 457—465. https://doi.org/10.1016/j.ecss.2007.07.020

Paytan, A., Shellenbarger, G.G., Street, J.J., Davis, K., Young, M.B., Moore, W.S., 2006. Submarine groundwater discharge: An important source of new inorganic nitrogen to coral reef ecosystems. Limnol. Oceanogr. 51 (1), 343—348. https://doi.org/10.4319/lo.2006.51.1.0343

Peltonen, K., 2002. Direct Groundwater Inflow to the Baltic Sea. TemaNord, Nordic Councils of Ministers, Copenhagen, the Netherlands, 79 pp.

Piekarek-Jankowska, H., 1994. Zatoka Pucka jako Obszar Drenażu Wód Podziemnych. Rozp. Monogr., Wyd. UG, Gdańsk 31—32, 204.
Piekarek-Jankowska, H., 1996. Hydrochemical effects of submarine groundwater discharge to the Puck Bay (Southern Baltic Sea, Poland). Geographia Polonica 67.
Povinec, P.P., Bokuniewicz, H., Burnett, W.C., Cable, J., Charette, M., Comanducci, J-F., Kontar, E.A., Moore, W.S., Oberdorfer, J.A., de Oliveira, J., Peterson, R., Stieglitz, T., Taniguchi, M., 2008. Isotope tracing of submarine groundwater discharge offshore Ubatuba, Brazil: results of the IAEA-Unesco SGD project. J. Environ. Radioactiv. 99, 1596—1610. https://doi.org/10.1016/j.jenvrad.2008.06.010
Purkamo, L., von Ahn, C.M.E., Jilbert, T., Muniruzzaman, M., Bange, H.W., Jenner, A-K., Böttcher, M.E., Virtasalo, J.J., 2022. Impact of submarine groundwater discharge on biogeochemistry and microbial communities in pockmarks. Geochim. Cosmochim. Ac. 334, 14—44. https://doi.org/10.1016/j.gca.2022.06.040
Purkl, S., Eisenhauer, A., 2004. Determination of radium isotopes and ^{222}Rn in a groundwater affected coastal area of the Baltic Sea and the underlying sub-sea floor aquifer. Mar. Chem. 87, 137—149. https://doi.org/10.1016/j.marchem.2004.02.005
Qian, Q., Clark, J.J., Voller, V.R., Stefan, H.G., 2009. Depth-dependent dispersion coefficient for modeling of vertical solute exchange in a lake bed under surface waves. J. Hydraul. Eng. 135 (3), 187—197. https://doi.org/10.1061/(ASCE)0733-9429(2009)135:3(187)
R Core Team. R: a language and environment for statistical computing. In: R Foundation for Statistical Computing. Austria, Vienna.
Racasa, E.D., Lennartz, B., Toro, M., Janssen, M., 2021. Submarine Groundwater Discharge From Non- Tidal Coastal Peatlands Along the Baltic Sea. Front. Earth. Sci. 9, 665802. https://doi.org/10.3389/feart.2021.665802
Rodellas, V., Garcia-Orellana, J., Garcia-Solsona, E., Masque, P., Dominguez, J.A., Ballesteros, B.J., Mejias, M., Zarroca, M., 2012. Quantifying groundwater discharge from different sources into a Mediterranean wetland by using ^{222}Rn and Ra isotopes. J. Hydrol. 466-467, 11—22. https://doi.org/10.1016/j.jhydrol.2012.07.005
Rodellas, V., Garcia-Orellana, J., Trezzi, G., Masque, P., Stieglitz, T.C., Bokuniewicz, H., Cochran, J.K., Berdalet, E., 2017. Using the radium quartet to quantify submarine groundwater discharge and porewater exchange. Geochim. Cosmochim. Ac. 196, 58—73. https://doi.org/10.1016/j.gca.2016.09.016
Sadat-Noori, M., Maher, D.T., Santos, I.R., 2016. Groundwater Discharge as a Source of Dissolved Carbon and Greenhouse Gases in a Subtropical Estuary. Estuar. Coast. 36, 639—656. https://doi.org/10.1007/s12237-015-0042-4
Santos, I.R., Eyr, B.D., Huette, M., 2012. The driving forces of porewater and groundwater flow in permeable coastal sediments: A review. Estuar. Coast. Shelf Sci. 98, 1—15. https://doi.org/10.1016/j.ecss.2011.10.024
Santos, I.R., Chen, X., Lecher, A.L., Sawyer, A.H., Moosdorf, N., Rodellas, V., Tamborski, J., Cho, H-M., Dimova, N., Sugimoto, R., Bonaglia, S., Li, H., Hajati, M-C., Li, L., 2021. Submarine groundwater discharge impacts on coastal nutrient biogeochemistry. Nat. Rev. Earth Environ. 2, 307—323. https://doi.org/10.1038/s43017-021-00152-0
Schlitzer, R., 2001. Ocean Data View available at:. http://www.awi-bremerhaven.de/GEO/ODV.
Schlüter, M., Sauter, E., Andersen, C.E., Dahlgaard, H., Dando, P.R., 2004. Spatial Distribution and Budget for Submarine Groundwater Discharge in Eckernförde Bay (Western Baltic Sea). Limnol. Oceanogr. 49, 157—167. https://doi.org/10.4319/lo.2004.49.1.0157
Seeberg-Elverfeldt, J., Schlüter, M., Feseker, T., Kölling, M., 2005. Rhizon sampling of porewaters near the sediment-water interface of aquatic systems. Limnol. Oceanogr.-Meth. 3, 361—371. https://doi.org/10.4319/lom.2005.3.361
Slomp, C., Van Cappellen, P., 2004. Nutrients inputs to the coastal ocean through submarine groundwater discharge: controls and potential impact. J. Hydrol. 295, 64—86. https://doi.org/10.1016/j.jhydrol.2004.02.018
Soetaert, K., Meysman, F., 2012. Reactive transport in aquatic ecosystems: Rapid model prototyping in the open source software R. Environ. Modell. Softw. 32, 49—60. https://doi.org/10.1016/j.envsoft.2011.08.011
Strady, E., Pohl, C., Yakushev, E.V., Krüger, S., Hennings, U., 2008. Pump-CTD-System for trace metal sampling with a high vertical resolution. A test in the Gotland Basin, Baltic Sea. Chemosphere 70, 1309—1319. https://doi.org/10.1016/j.chemosphere.2007.07.051
Sültenfuß, J., Rhein, M., Roether, W., 2009. The Bremen mass spectrometric facility for the measurement of helium isotopes, neon and tritium in water. Isot. Environ. Health. S. 45 (2), 1—13. https://doi.org/10.1080/10256010902871929
Szymczak, E., Piekarek-Jankowska, H., 2007. The transport and distribution of the river load from the Reda River into the Puck Lagoon (southern Baltic Sea, Poland). Oceanol. Hydrobiol. St. XXXVI, 103—124. https://doi.org/10.2478/v10009-007-0012-7
Szymczak, E., Szmytkiewicz, A., 2014. Sediment deposition in the Puck Lagoon (Southern Baltic Sea, Poland). BALTICA 27, 105—118. https://doi.org/10.5200/baltica.2014.27.20
Szymczycha, B., Böttcher, M.E., Diak, M., Koziorowska-Makuch, K., Kuliński, K., Makuch, P., von Ahn, C.M.E., Winogradow, A., 2023. The benthic-pelagic coupling affects the surface water carbonate system above groundwater-charged coastal sediments. Front. Mar. Sci. 10, 1218245. https://doi.org/10.3389/fmars.2023.1218245
Szymczycha, B., Klostowska, Z., Lengier, M., Dzierzbicka-Glowacka, L., 2020. Significance of nutrients fluxes via submarine groundwater discharge in the Bay of Puck, southern Baltic Sea. Oceanologia 62 (2), 117—125. https://doi.org/10.1016/j.oceano.2019.12.004
Szymczycha, B., Vogler, S., Pempkowiak, J., 2012. Nutrient fluxes via submarine groundwater discharge to the Bay of Puck, southern Baltic Sea. Sci. Total. Environ. 438, 86—93. https://doi.org/10.1016/j.scitotenv.2012.08.058
Szymczycha, B., Kroeger, K.D., Pempkowiak, J., 2016. Significance of groundwater discharge along the coast of Poland as a source of dissolved metals to the southern Baltic Sea. Mar. Pollut. Bull. 109, 151—162. https://doi.org/10.1016/j.marpolbul.2016.06.008
Szymczak-Zyla, M., Lubecki, L., 2022. Biogenic and anthropogenic sources of sedimentary organic matter in marine coastal areas. A multi-proxy approach based on bulk and molecular markers. Mar. Chem. 239, 104069. https://doi.org/10.1016/j.marchem.2021.104069
Stosch, H.-G., 2022. Excel template to plot hydrochemical data into a Piper diagram (1.0). Zenodo. doi:10.5281/zenodo.5994293.
Tamborski, J., Bejannin, S., Garcia-Orellana, J., Souhaut, M., Charbonnier, C., Anschutz, P., Pujo-Pay, M., Conan, P., Crispi, O., Monnin, C., Stieglitz, T., Rodellas, V., Andriosa, A., Claude, C., van Beek, P., 2018. A comparison between water circulation and terrestrially-driven dissolved silica fluxes to the Mediterranean Sea traced using radium isotopes. Geochim. Cosmochim. Ac. 238, 496—515. https://doi.org/10.1016/j.gca.2018.07.022
Tamisier, M., Schmidt, M., Vogt, C., Kümmel, S., Stryhanyuk, H., Musat, N., Richnow, H.-H., Musat, F., 2022. Iron corrosion by methanogenic archaea characterized by stable isotope effects and crust mineralogy. Environ. Microbiol. 24 (2), 583—595. https://doi.org/10.1111/1462-2920.15658
Taniguchi, M., Burnett, W.C., Cable, J.E., Turner, J.V., 2002. Inves-

tigation of submarine groundwater discharge. Hydrol. Proc. 16, 2115—2129. https://doi.org/10.1002/hyp.1145

Taniguchi, M., Dulaim, H., Burnett, K.M., Santos, I.R., Sugimoto, R., Stieglitz, T., Kim, G., Moosdorf, N., Burnett, W., 2019. Submarine Groundwater Discharge Updates on its Measurement Techniques, Geophysical Drivers, Magnitudes, and Effects. Front. Environ. Sci. 7, 141. https://doi.org/10.3389/fenvs.2019.00141

Top, Z., Brand, L.E., Corbett, R.D., Burnett, W., Chanton, J., 2001. Helium and radon as tracers of groundwater input into Florida Bay. J. Coast. Res. 17 (4), 859—868. http://www.jstor.org/stable/4300245.

Thang, N.M., Brüchert, V., Formolo, M., Wegener, G., Ginters, L., Jørgensen, B.B., Ferdelman, T.G., 2013. The Impact of Sediment and Carbon Fluxes on the Biogeochemistry of Methane and Sulfur in Littoral Baltic Sea Sediments (Himmerfjärden, Sweden). Estuar. Coast. 36, 98—115. https://doi.org/10.1007/s12237-012-9557-0

Van den Berg, C.M.G., Rogers, H., 1987. Determination of alkalinities of estuarine waters by a two-point potentiometric titration. Mar. Chem. 20, 219—226. https://doi.org/10.1016/0304-4203(87)90073-9

Virtasalo, J.J., Schroeder, J.F., Luoma, S., Majaniemi, J., Mursu, J., Scholten, J., 2019. Submarine Groundwater Discharge Site in the First Salpausselkä Ice-Marginal Formation, South Finland. Solid Earth-EGU 10, 405—432. https://doi.org/10.5194/se-10-405-2019

Viventsowa, E.E., Voronov, A.N., 2003. Groundwater discharge to the Gulf of Finland (Baltic Sea): ecological aspects. Environ. Geol. 45, 221—225. https://doi.org/10.1007/s00254-003-0869-z

von Ahn, C.M.E., Scholten, J.C., Malik, C., Feldens, P., Liu, B., Dellwig, O., Jenner, A-K., Papenmeier, S., Schmiedinger, I., Zeller, M.A., Böttcher, M.E., 2021. A multi-tracer study of freshwater sources for a temperate urbanized coastal bay (Southern Baltic Sea). Front. Environ. Sci. 9, 642346. https://doi.org/10.3389/fenvs.2021.642346

Winde, V., Böttcher, M.E., Escher, P., Böning, P., Beck, M., Liebezeit, G., Schneider, B., 2014. Tidal and spatial variations of $DI^{13}C$ and aquatic chemistry in a temperate tidal basin during winter time. J. Marine Syst. 129, 394—402. https://doi.org/10.1016/j.jmarsys.2013.08.005

Whiticar, M.J., Werner, F., 1981. Pockmarks: Submarine Vents of Natural Gas or Freshwater Seeps? Geo-Mar. Lett. 1, 193—199. https://doi.org/10.1007/BF02462433

Whiticar, M.J., Faber, E., 1986. Methane oxidation in sediment and water column environments — Isotope evidence. Adv. Org. Geochem. 10, 759—768. https://doi.org/10.1016/S0146-6380(86)80013-4

Whiticar, M.J., 1999. Carbon and hydrogen isotope systematics of bacterial formation and oxidation of methane. Chem. Geol. 161, 291—314. https://doi.org/10.1016/S0009-2541(99)00092-3

Zektzer, I.S., Ivanov, V.A., Meskheteli, A.V., 1973. The problem of direct groundwater discharge to the seas. J. Hydrol. 20, 1—36. https://doi.org/10.1016/0022-1694(73)90042-5